

Original Article

Cite this article: Skoblenko (Pilitsyna) AV, Kanygina NA, Dubenskiy AS, Batanova VG, Dilek Y, Sheshukov VS, and Serov PA (2023) High-pressure metamorphism of Precambrian continental crust in the southwestern part of the Central Asian Orogenic Belt (South Kazakhstan and North Tien Shan) and tectonic implications for the evolution of the Palaeo-Asian Ocean. *Geological Magazine* **160**: 1624–1648. <https://doi.org/10.1017/S0016756823000626>

Received: 14 May 2023

Revised: 18 September 2023

Accepted: 25 September 2023

Keywords:


Central Asian Orogenic Belt; high-pressure metamorphism; Precambrian; early Palaeozoic; continental crust; zircon dating; phase diagram modelling; Palaeo-Asian Ocean

Corresponding author:

Anfisa V. Skoblenko;

Email: an.pilitsyna@gmail.com

High-pressure metamorphism of Precambrian continental crust in the southwestern part of the Central Asian Orogenic Belt (South Kazakhstan and North Tien Shan) and tectonic implications for the evolution of the Palaeo-Asian Ocean

Anfisa V. Skoblenko (Pilitsyna)¹ , Nadezhda A. Kanygina¹, Alexander S. Dubenskiy¹, Valentina G. Batanova², Yildirim Dilek³, Victor S. Sheshukov¹ and Pavel A. Serov⁴

¹Geological Institute, Russian Academy of Sciences, Pyzhevsky lane, 7a, Moscow, Russia; ²University of Grenoble Alpes, Univ. Savoie Mont Blanc, CNRS, IRD, IFSTTAR, ISTERRE, 38000 Grenoble, France; ³Department of Geology and Environmental Earth Science, Miami University, Oxford, OH 45056, USA and ⁴Geological Institute of the Kola Science Centre, Russian Academy of Sciences, 184209 Apatity, Russia

Abstract

In this study, we investigated the high-pressure (HP) metamorphism of the Precambrian continental crust exposed in the Zheltau terrane in South Kazakhstan (Koyandy complex) and the Chu-Kendykta terrane in the North Tien Shan of Kyrgyzstan (Aktyuz, Kemin and Kokdzhon complexes) within the SW part of the Central Asian Orogenic Belt. HP quartz–feldspar lithologies of the Koyandy complex consist of migmatized kyanite-bearing garnet–mica paragneisses, garnet–kyanite paragneisses and their derivatives associated with eclogites. Paragneisses demonstrate prograde evolution involving mica dehydration melting and producing magnesium-rich garnet, kyanite and K-feldspar at the near-peak to retrograde stages at pressures of 15–18.5 kbar and temperatures of 800–870°C. The widespread growth of micas in these rocks reflects lower stages of retrogression at $P = 10\text{--}12$ kbar and $T = 720\text{--}770^\circ\text{C}$. The age distributions of the cores of detrital zircon grains from the paragneisses indicate a predominance of Neoproterozoic and minor occurrence of Mesoproterozoic and Palaeoproterozoic sources of their protoliths. The ages of ~487–485 Ma obtained from the zircon rims of the paragneisses reflect the timing of their HP metamorphic re-equilibration. These age clusters are consistent with the age estimates obtained from the rims of zircons in the eclogite-bearing garnet gneisses of the adjacent Aktyuz complex in the North Tien Shan. The $P\text{--}T$ paths and zircon ages obtained from the high-grade quartz–feldspar gneisses of the Zheltau and Chu-Kendykta terranes are thus interpreted to indicate involvement of the crustal material derived from the Precambrian basement (magmatic zircons aged ca. 844 Ma) and its Ediacaran–Cambrian sedimentary cover (detrital zircons with maxima at 1 Ga and 800–600 Ma) in the latest Cambrian subduction processes induced by the closure of the oceanic basins assigned to the Palaeo-Asian Ocean.

1. Introduction

The Central Asian Orogenic Belt (CAOB) represents the largest accretionary orogen in the world (Figure 1(a)) and is delimited by the Siberian, North China and Tarim cratons that extend through the territories of the Urals, Kazakhstan, Tien Shan, northwestern China, Mongolia and Southern Siberia. The CAOB displays a prolonged tectonic history of development from the Neoproterozoic to the early Mesozoic that involved a series of accretionary events during the evolution of the Palaeo-Asian Ocean (Windley *et al.* 2007; Yarmolyuk & Degtyarev, 2019). The formation of a vast volume of continental crust within the CAOB took place largely during the Precambrian (mostly Palaeo- and Mesoproterozoic) and in part during the early Palaeozoic (Kröner *et al.* 2014, 2017a; Degtyarev *et al.* 2017). Consequently, the CAOB contains large domains of low- to moderate-grade metamorphosed Precambrian crustal rocks (gneissic granites, orthogneisses and felsic metavolcanic rocks).

In the study area of the southwestern segment of the CAOB, Precambrian metamorphic complexes are commonly associated with high- and ultrahigh-pressure (HP–UHP) rocks, which are mainly eclogites and garnet-bearing gneisses (HP granulites). These high-grade rocks were derived from the reworking of Precambrian crust in subduction zones during the Cambrian–Early Ordovician, when different oceanic basins of the Palaeo-Asian Ocean were closed (e.g. Kröner *et al.* 2012; Konopelko *et al.* 2012; Konopelko & Klemd, 2016; Pilitsyna *et al.* 2019). The HP–UHP formations known from the Issyk-Kul terrane (Makbal ultrahigh-pressure (UHP)

© The Author(s), 2023. Published by Cambridge University Press. This is an Open Access article, distributed under the terms of the Creative Commons Attribution licence (<http://creativecommons.org/licenses/by/4.0/>), which permits unrestricted re-use, distribution and reproduction, provided the original article is properly cited.



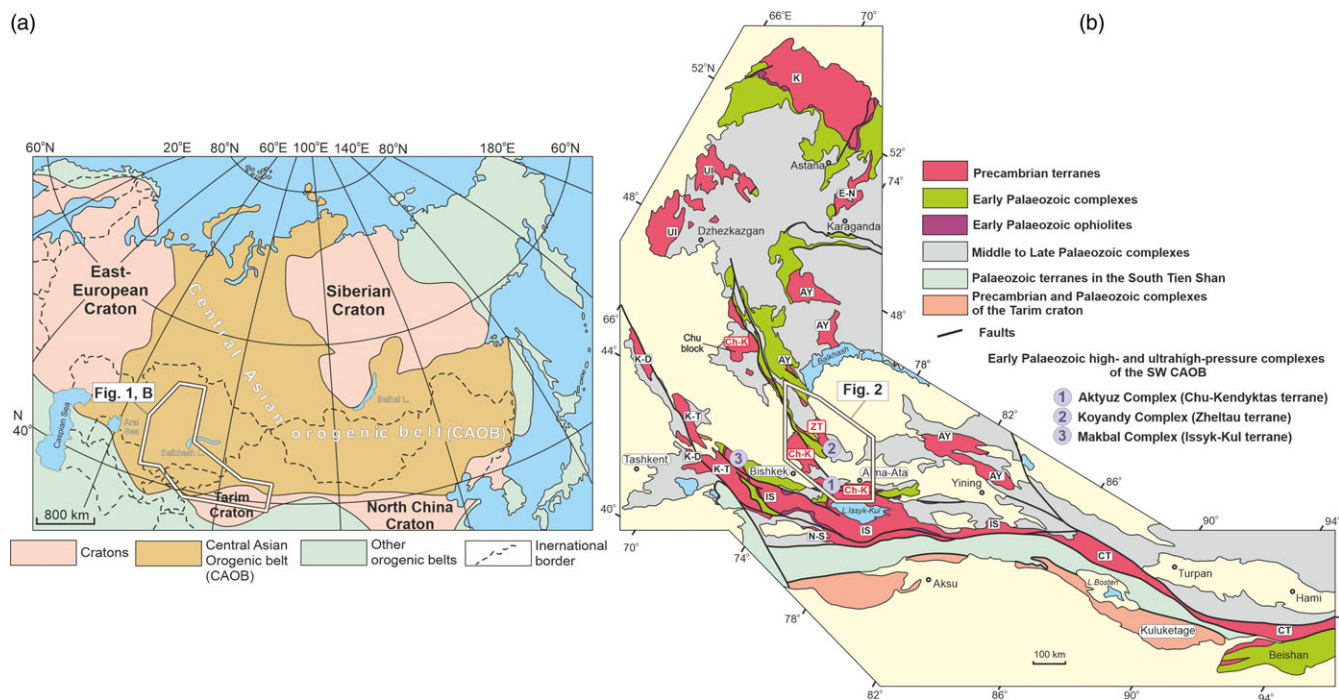


Figure 1. (Colour online) (a) Location of the Central Asian Orogenic Belt (CAOB) in North Eurasia (after Degtyarev *et al.* 2021); (b) Precambrian terranes distributed within the western segment of the CAOB: AY – Aktau-Yili, CT – Chinese Central Tien Shan, E-N – Erementau-Niyaz, IS – Issyk-Kul, K – Kokchetav, ZT – Zheltau, Ch-K – Chu-Kendykta, K-D – Karatau-Dzhebagly, K-T – Karatau-Talas, N-S – Naryn-Sarydzhas, Ul – Ulutau (after Degtyarev *et al.* 2017).

complex; North Tien Shan), Chu-Kendykta terrane (Aktuz HP complex; North Tien Shan) and Zheltau terrane (Koyandy HP complex; South Kazakhstan) have been the main focus of many studies aimed at estimating the timing, parameters and settings of the metamorphism of Precambrian continental crust and comparing these data with the extant results of investigations of eclogites from HP–UHP metamorphic complexes.

Here, we report new data on the ages of the HP paragneisses of the Koyandy complex (Zheltau terrane; South Kazakhstan), elucidate the P–T evolution of these rocks and correlate our results with those reported previously from the adjacent Aktuz complex (Chu-Kendykta terrane; North Tien Shan). We also discuss the Precambrian tectonic affinities of the protoliths of the studied HP paragneisses in the Koyandy complex and similar formations of the adjacent terranes and their late Cambrian–Early Ordovician metamorphic evolution. In the last part of the paper, we evaluate the existing geodynamic models of the early Palaeozoic evolution of HP–UHP rock assemblages in the southwestern segment of the CAOB in light of our new data reported in this study.

2. Geological background

The crustal makeup of the CAOB includes blocks of Precambrian crust of variable sizes and fragments of island arc and ophiolite fragments preserved within early Palaeozoic accretionary prism complexes (Yarmolyuk & Degtyarev, 2019). In the western part of the CAOB exposed in Kazakhstan, Tien Shan and Northwestern (NW) China, Precambrian terranes occur as narrow tectonic zones that are several hundred km long and 50 to 100 km wide (Figure 1(b)). These Precambrian terranes commonly contain a basement composed of strongly to moderately deformed and metamorphosed Meso- and Neoproterozoic granitoids and/or

felsic volcanic rocks (gneissic granites and orthogneisses). These crystalline rocks are covered by weakly deformed sedimentary cover consisting mainly of Ediacaran–Cambrian quartzites and shales (Degtyarev *et al.* 2017; Kanygina *et al.* 2021; Skoblenko *et al.* 2022). Extant geochronological and Sm–Nd isotope data show that the majority of the granitoids in the basement were derived from partial melting of an early Precambrian continental crust; juvenile crustal material contribution to the magmatic evolution of these granitoids was minimal (e.g. Kröner *et al.* 2012, 2013; Degtyarev *et al.* 2017; Kovach *et al.* 2017).

In the southwestern (SW) part of the CAOB, the Precambrian crust exposed in the Zheltau and Chu-Kendykta terranes in South Kazakhstan and in the North Tien Shan and in the Issyk-Kul terrane in the North Tien Shan (Figure 1(b)) is composed of metamorphosed Palaeo-, Meso- and Neoproterozoic felsic rocks (Degtyarev *et al.* 2011, 2017; Kröner *et al.* 2007, 2012, 2013; Pilityna *et al.* 2019; Skoblenko *et al.* 2022; Kushnareva *et al.* 2022). HP–UHP rocks corresponding to variously retrograded eclogites and garnet-bearing quartz–feldspar gneisses (\pm coesite) are also common occurrences in these terranes and are interpreted to have originated from the subduction of Precambrian continental crust in the early Palaeozoic (509–474 Ma) during the closure stages of the Palaeo-Asian Ocean (e.g. Alexeiev *et al.* 2011; Kröner *et al.* 2012; Rojas-Agramonte *et al.* 2013; Klemd *et al.* 2014; Konopelko & Klemd, 2016; Pilityna *et al.* 2018a, 2019). The HP–UHP rock assemblages were then exhumed from different structural depths, forming tectonic slices of various metamorphosed formations. Within the study area, these HP–UHP rocks are assigned to the Makbal (Issyk-Kul terrane), Aktuz (Chu-Kendykta terrane) and Koyandy complexes (Figure 1(b)). The formation of these complexes is thought to have been related to the evolution of the early Palaeozoic Dzhair-Naiman and Kara-Archa ophiolite zones.

2.1. Makbal ultrahigh-pressure complex (Issyk-Kul terrane)

The UHP formations within the Issyk-Kul terrane in the North Tien Shan are represented by eclogites and amphibolites (formed after eclogites), as well as coesite-bearing garnet–chloritoid–talc schists and coesite-bearing garnet quartzites of the Makbal complex. The UHP rocks of the Makbal complex are juxtaposed against quartzites and mica schists of lower grades. The protoliths of the eclogites are considered either palaeo-oceanic crust or mafic dikes emplaced into continental crust prior to UHP metamorphism during the final stages of Rodinia breakup (Meyer *et al.* 2014; Rojas-Agramonte *et al.* 2013). The timing of the near-peak-stage metamorphism of the eclogites has been generally interpreted as ~509–498 Ma based on U–Pb dating of zircon rims (Konopelko *et al.* 2012), although a Lu–Hf garnet-whole rock isochron yields a younger age of ca. 470 Ma for this HP metamorphism (Rojas-Agramonte *et al.* 2013). Some of the crustal rocks of the Makbal complex have experienced UHP re-equilibration at >24 kbar (Tagiri & Bakirov, 1990; Meyer *et al.* 2014). Zircon rims from the garnet–chloritoid–talc schists have yielded a U–Pb mean age of ca. 502 Ma for the UHP event, whereas zircon core ages cover a wide range from 2,583 to 642 Ma. This wide age span may indicate the sedimentary origin of the protolith rocks (Konopelko *et al.* 2012, Konopelko & Klemd, 2016). The negative ϵ_{Nd} = –11 values (Meyer *et al.* 2014) of the garnet–chloritoid–talc schists suggest that ancient crustal material was an essential component of their protoliths. Protoliths of coesite-bearing garnet quartzites of the Makbal complex were similarly made of terrigenous strata, the accumulation of which occurred in a passive margin setting (Togonbaeva *et al.* 2009; Konopelko & Klemd, 2016). Neoproterozoic and Palaeoproterozoic crustal material (2.7–1.6 Ga) was the main source of the protoliths of quartzites (Degtyarev *et al.* 2013; Konopelko & Klemd, 2016; Alexeiev *et al.* 2020).

2.2. Aktyuz high-pressure complex (Chu-Kendykta terrane)

Late Tonian medium-grade gneissic granites and orthogneisses (~840–780 Ma) and variously altered Cambrian paragneisses with low-grade mica schists make up much of the Aktyuz, Kemin and Kokdzhon complexes in the SE part of the Chu-Kendykta terrane in the North Tien Shan (Figure 2) (Kröner *et al.* 2012; Rojas-Agramonte *et al.* 2014; Skoblenko *et al.* 2023). Magmas of the Neoproterozoic granitoids were derived from partial melting of early Precambrian crustal material with model Nd ages of 2.1–1.5 Ga (Kröner *et al.* 2012). These Neoproterozoic granitoids constitute the basement of the Chu-Kendykta terrane. The Aktyuz complex includes eclogite that is spatially associated with quartz–feldspar garnet–mica gneisses and their lower-grade derivatives. Lu–Hf garnet isochron dating of the amphibolised eclogite yields an age of ca. 474 Ma, which has been interpreted as the timing of their near-peak stage of HP metamorphism. The protolith of this eclogitic rock was rifting-derived mafic dikes that intruded into the continental crust sequence prior to the late Cambrian–Early Ordovician subduction stage (Rojas-Agramonte *et al.* 2014; Klemd *et al.* 2014). On the other hand, zircons separated from the associated HP garnet–mica gneisses have yielded two age clusters, corresponding to the timing of the HP re-equilibration at ca. 490 Ma and the protolith age of ca. 844 Ma known from the inherited zircon cores (Skoblenko *et al.* 2023). Detrital zircon populations from the paragneisses and schists of the Kokdzhon and Kemin complexes of the Chu-Kendykta terrane show wide age ranges for the cores (at 600, 800 and 1000 Ma and less than 1.5 and 2.5 Ga) and varisized rims aged 495–471 Ma,

compatible with the near-peak to retrograde metamorphic evolution of the metasedimentary rocks (Skoblenko *et al.* 2023).

2.3. Koyandy high-pressure complex (Zheltau terrane)

Prevailing metamorphic formations in the basement of the Zheltau terrane in South Kazakhstan consist mainly of Palaeoproterozoic (ca. 1840 Ma) and Neoproterozoic (ca. 790 Ma) orthogneisses with amphibolites (\pm garnet) derived from early Precambrian crustal sources with estimated Nd model ages of 2.3–2.1 Ga (Pilitsyna *et al.* 2019; Skoblenko *et al.* 2022) (Figure 2). Ediacaran–Cambrian metasedimentary formations take up much less space in the Koyandy complex and are composed mainly of low-grade two-mica or chloritized schists, quartzites and marbles, associated with variously retrograded kyanite-bearing garnet–mica gneisses and schists (Figure 3). The latter commonly contains tectonic lenses and boudins of eclogites intercalated with garnet pyroxenites, garnet amphibolites formed after eclogites and rare serpentinitized symplectite-bearing peridotites, which record HP near-peak stages of at least $P = 16$ – 18 kbar during their evolution (Pilitsyna *et al.* 2018a, b). A U–Pb zircon age of ca. 490 Ma was obtained from the garnet pyroxenites of the Koyandy complex (Alexeiev *et al.* 2011), corresponding to the timing of their HP metamorphism. In turn, the protoliths of the eclogites and garnet pyroxenites are interpreted to have been derivatives of intraplate mafic melts that intruded into continental crust before the onset of subduction (Pilitsyna *et al.* 2018a). Protoliths of metasedimentary garnet–mica schists exposed in the central part of the Anrakhai Block (Figure 3) are terrigenous rocks with main age peaks at ~991 Ma and ~1082 Ma and, to a lesser extent, 1.6–1.8 Ga and ~2.5 Ga (Pilitsyna *et al.* 2019). One of the detrital zircon grain rims obtained from these schists revealed an age of ~486 Ma from its rims, indicating that the protoliths of these rocks might have experienced subduction zone processes.

In the SE part of the Anrakhai Block of the Zheltau terrane (Figure 3(a)), quartz–feldspar migmatized gneisses (Figure 3(b)) are spatially associated with metre-scale eclogitic boudins (Figure 3(c)). One of these migmatitic gneiss exposures contains distinctive bands of melanosomes composed of garnet–mica gneisses with kyanite and leucosome bands of weakly deformed granitoid gneisses (Figure 3(d)–(e)). Exposures of strongly foliated, coarse-grained garnet–kyanite schists (retrograded paragneisses) crop out in the vicinity of migmatitic gneiss with eclogites (Figure 4). These rocks have been interpreted to represent HP felsic granulites formed at a near-peak stage of metamorphism at pressures of 15–18 kbar and temperatures of 750–850°C (Pilitsyna *et al.* 2019).

3. Methods

3.1. Whole-rock and mineral chemistry analyses

X-ray fluorescence (XRF) was used to determine the major elements using a Bruker AXS wavelength dispersive S4 PIONEER spectrometer with a 4-kW X-ray tube at the Geological Institute of the Russian Academy of Sciences (RAS). The Spectra-Plus software package was used for data processing. The automatic registration of peak overlaps and correction for matrix effects were performed during individual measurements of fundamental parameters for each sample. The intervals of analyzed concentrations obtained after re-calculation to oxides (mass fraction %) were as follows: Si = 0.01–1.0, Ti = 0.01–5.0, Al = 1.0–60.0, Fe (total) = 1.0–40.0, Mn = 0.01–1.0, Ca = 1.0–50, Mg = 0.1–40, Na = 0.1–10.0, K = 0.1–10.0 and P = 0.01–5.0. The contents of FeO were

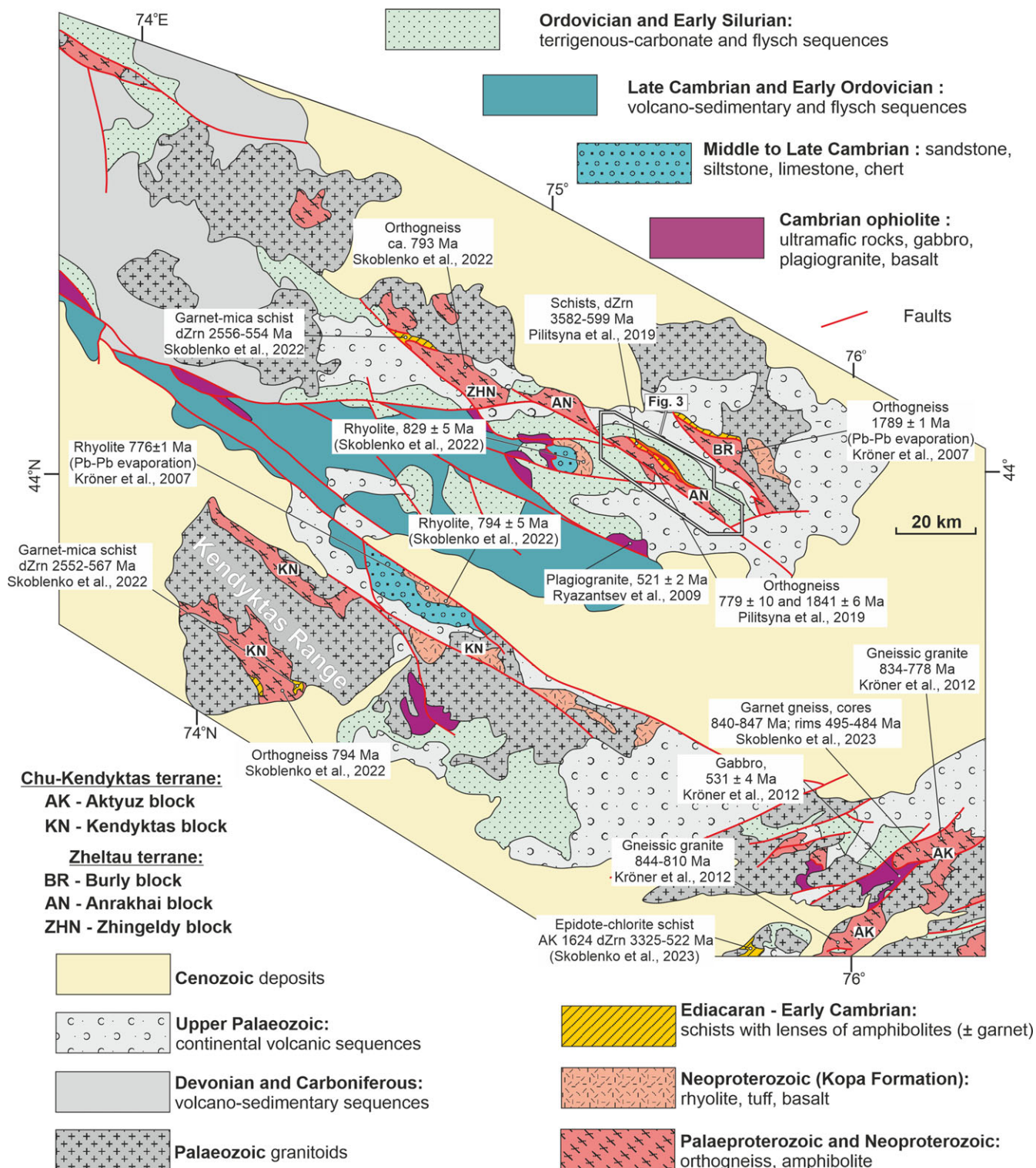


Figure 2. (Colour online) Geological map of the SE part of the Chu-Kendykta (North Tien Shan) and Zheltau (South Kazakhstan) terranes. Age estimates for the principal rock types are after Kröner *et al.* (2007, 2012), Ryazantsev *et al.* (2009), Pilitsyna *et al.* (2019) and Skoblenko *et al.* (2022, 2023).

determined by wet chemistry via titration with potassium dichromate in sulphuric acid medium after acid decomposition of the sample in the absence of oxygen at the Geological Institute RAS. To obtain the contents of Fe(III) in the form of Fe₂O₃, the XRF data was corrected for the amount of iron (II) oxide obtained from the results of titration.

Whole-rock trace element analysis was performed at the Analytical Centre of the Institute of Microelectronics Technology, Moscow, and High-Purity Materials, RAS, using a PerkinElmer ELAN 6100 DRC inductively coupled plasma mass spectrometer (ICP-MS) and atomic emission spectrometry with an ICP-MS (ICAP-61, Thermo Jarrell Ash; X-7, Thermo Elemental, USA). The

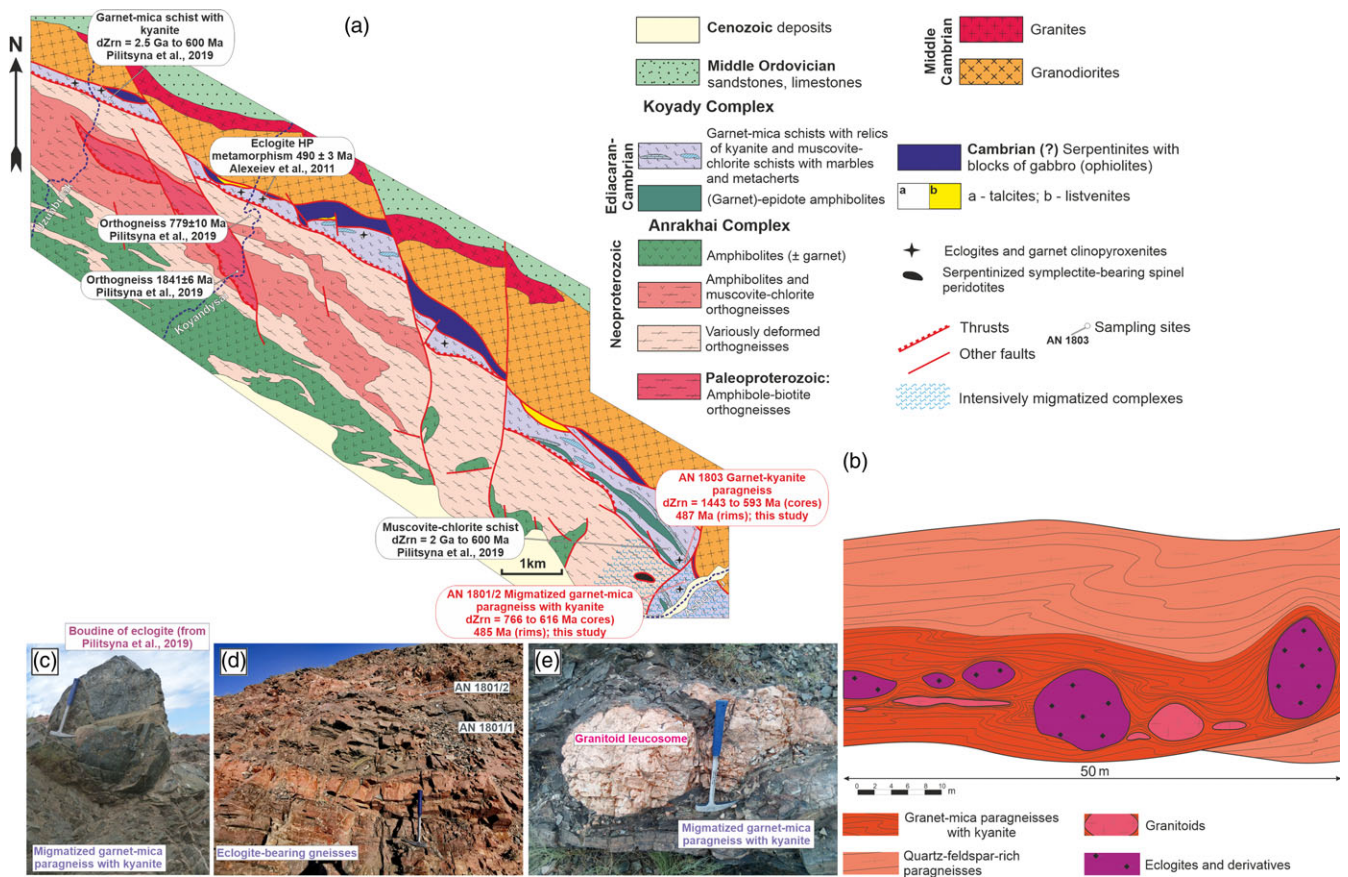


Figure 3. (Colour online) Geological map of the Anrakhai Block (Zheltau terrane). Age estimates for the principal rock types of the Anrakhai and Koyandy metamorphic complexes are after Alexeiev *et al.* (2011) and Pilitsyna *et al.* (2019).

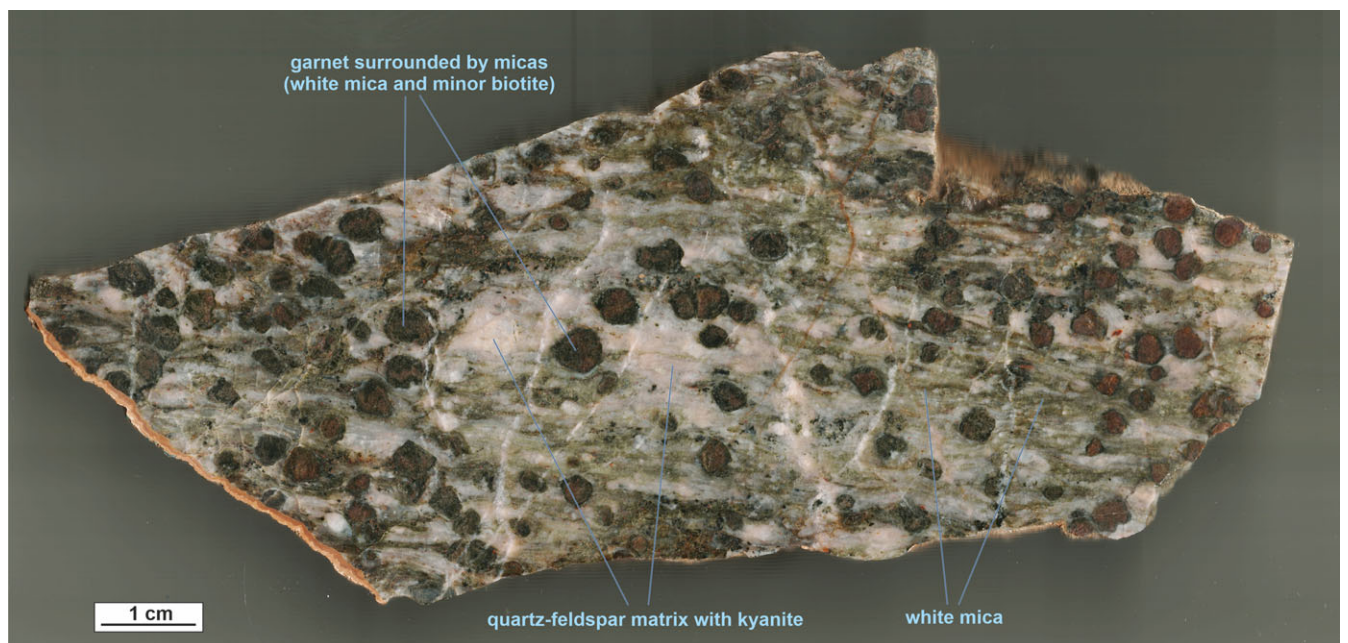


Figure 4. (Colour online) Scanned photograph of a polished sample of garnet-kyanite schist (retrograded paragneiss) AN1803 from the Koyandy complex (Zheltau terrane).

relative standard deviations for all analyzed elements were not more than 0.2 for element contents below the five-fold detection limit and below 0.1 for contents above this detection limit. The major elements and trace elements concentrations are presented in wt.% and ppm, respectively.

Mineral compositions and element maps were obtained using JEOL JXA-8230 and JXA-iHP200F EPMA at the Institut des Sciences de La Terre (ISTerre, University Grenoble Alpes, France), equipped with five wavelength dispersive spectrometers and an energy dispersive (EDX) spectrometer operating at 20 kV accelerating voltage, 20 nA probe current and 1 μm beam diameter. Mineral compositions of the sample AK1904 were obtained using a JSM-6510 scanning electron microscope with an EDX INCA Energy-350 (Oxford Instruments) and MIRA 3 (TESCAN, Czech Republic) at the Analytical Center of Geological Institute RAS.

Fe^{3+} was recalculated for garnet based on charge balance and stoichiometry. Mineral abbreviations are after Whitney & Evans (2010); a.p.f.u. is atom per formula unit.

3.2. SHRIMP II U-Pb isotope analyses

A SHRIMP II ion probe was used for zircon dating at the Center for Isotopic Research at the Karpinsky Russian Geological Research Institute (Saint Petersburg, Russia) following conventional techniques (Williams, 1998; Larionov *et al.* 2004). The zircons were mounted in epoxy along with the zircon standards 91500 (Wiedenbeck *et al.* 1995) and Temora (Black *et al.* 2003), polished to approximately half of the grain thickness and coated with 99.999% pure gold. Optical microscopy and cathodoluminescence were performed on euhedral crystals selecting the regions devoid of visible cracks and inclusions to investigate the inner structure of the zircons. Data were processed with SQUID v1.12 and ISOPLOT/Ex 3.22 (Ludwig, 2005a, b) using the decay constants of Steiger & Jäger (1976). Common Pb correction was applied based on the model by Stacey & Kramers (1975) using the measured $^{204}\text{Pb}/^{206}\text{Pb}$ ratio.

3.3. LA-ICP-MS U-Pb isotope analyses

U-Th-Pb zircon dating by LA-ICP-MS was carried out at the Geological Institute of RAS employing a sector field – inductively coupled plasma – mass spectrometer (SF-ICP-MS) Thermo-Scientific Element2 coupled to Electro Scientific NWR-213 laser ablation system (Sheshukov *et al.* 2018). Helium gas was used as the laser ablation carrier with further admixture of argon. Precise filtration and gas mixing were used to reduce gas noise and increase the stability of the analytical signal. The zircon reference material GJ-1 (Jackson *et al.* 2004; Elhlou *et al.* 2006) with accepted CA-ID-TIMS $^{206}\text{Pb}/^{238}\text{U}$ age of 601.9 ± 0.4 Ma (Horstwood *et al.* 2016) was used as a primary standard for external calibration procedure, provided by the Australian Research Council (ARC) National Key Centre for Geochemical Evolution and Metallogeny of Continents, Macquarie University (Sydney, Australia). For accuracy control, there were used 91500 (Wiedenbeck *et al.* 1995, 2004) and Plesovice (Sláma *et al.* 2008) zircon references with accepted CA-ID-TIMS $^{206}\text{Pb}/^{238}\text{U}$ ages 1063.5 ± 0.4 Ma and 337.2 ± 0.1 Ma, respectively (Horstwood *et al.* 2016). Glitter 4.4 software (Van Achterbergh *et al.* 2001) was used for data reduction and common lead correction was carried out using the T. Andersen procedure (Andersen, 2002) – ComPbCorr 3.18 software (Andersen, 2008). The Isoplot 4.15 software (Ludwig, 2008) and Isoplot R (Vermeesch, 2018) were used for graphic illustration of the results.

3.4. Sm-Nd isotope data

The Sm-Nd isotope research was carried out in the Collective Use Centre of the Kola Science Centre RAS (Apatity, Russia). The isotope Nd composition and Sm and Nd contents were measured by a 7-channel solid-phase mass-spectrometer, Finnigan-MAT 262, equipped with a Retarding Potential Quadrupole in a static double-band mode, using Ta + Re filaments. A mean value of $^{143}\text{Nd}/^{144}\text{Nd}$ ratio in a JNdi-1 standard was 0.512311 ± 7 ($N = 5$) in the test period. An error in $^{147}\text{Sm}/^{144}\text{Nd}$ in ratios was 0.3% (2σ), which is the mean value of seven measurements in a BCR-2 standard (Raczek *et al.* 2003). An error in the estimation of isotope Nd composition in an individual analysis was up to 0.004%. The blank intralaboratory contamination was 0.3 ng in Nd and 0.06 ng in Sm. The accuracy of the estimation of Sm and Nd contents was $\pm 0.5\%$. Isotope ratios were normalized per $^{146}\text{Nd}/^{144}\text{Nd} = 0.7219$, and then recalculated for $^{143}\text{Nd}/^{144}\text{Nd}$ in JNdi-1 = 0.512115 (Tanaka *et al.* 2000). Values of $\epsilon\text{Nd}(T)$ and $T(\text{DM})$ model ages were estimated using present-day values of CHUR as described in (Bouvier *et al.* 2008) ($^{143}\text{Nd}/^{144}\text{Nd} = 0.512630$, $^{147}\text{Sm}/^{144}\text{Nd} = 0.1960$) and DM as described in (Goldstein & Jacobsen, 1988) ($^{143}\text{Nd}/^{144}\text{Nd} = 0.513151$, $^{147}\text{Sm}/^{144}\text{Nd} = 0.2136$).

4. Results

4.1. Petrography, whole-rock and mineral chemistry of high-pressure metasedimentary rocks of the Koyandy complex

Metasedimentary rocks of the Koyandy complex in the Zheltau terrane consist of variously altered paragneisses and schists with different proportions of garnet, micas and feldspars relative to quartz. In the NW part of the Anrakhai Block (Figure 3(a)), mica-rich garnet schists form a narrow, 50–100 m-thick zone, whereas migmatized kyanite-bearing quartz–feldspar paragneisses and schists that are spatially associated with low-grade mica schists occur in the SE part of this block. The micaceous high-grade metasedimentary rocks contain pods and boudins of eclogites and garnet amphibolites formed after eclogites (Figure 3(c)), suggesting that HP rocks and metasedimentary rocks might have formed concurrently.

4.1.1. Migmatized garnet–mica paragneisses

These rocks contain intercalating bands of garnet–mica–feldspar–quartz–kyanite (melanosome) and granitoid leucosomes composed of feldspars, quartz and white mica (Figure 3(d)). The leucosomes also form injections and layers in the bands of dark garnet–mica gneisses (Figure 3(e)). Garnets in melanosome bands display euhedral or subhedral habits with partially preserved facets up to 0.5 mm in size (Figure 5(b) and (c); Figure 6(a)) and commonly contain inclusions of quartz, rutile and kyanite near their margins (Figure 5(a); Table S4). Garnets are characterized by pronounced chemical zoning with Mn-rich cores ($X_{\text{mn}} = 0.25$) and Ca-rich rims with Mg-rich rims (X_{ca} and X_{mg} correspond to 0.16 compared to $X_{\text{ca}} = 0.09$ and $X_{\text{mg}} = 0.15$ in the core) (Figure 6(a); Table S1). These zones show irregular diffusional boundaries (Figure 6(a)), which might indicate high-temperature modifications under increased P–T conditions. Feldspars of the melanosome matrix include plagioclase (oligoclase–andesine) and potassium feldspar (Table S2; Figure 5(e) and (f)), and together with quartz (up to 0.1 mm thick), they form ribbons in the direction of lineation in paragneisses (Figure 5(b)). Biotite and white mica grains are subparallel to lineation and are abundant in melanosomes in nearly equal proportions. Muscovite makes up

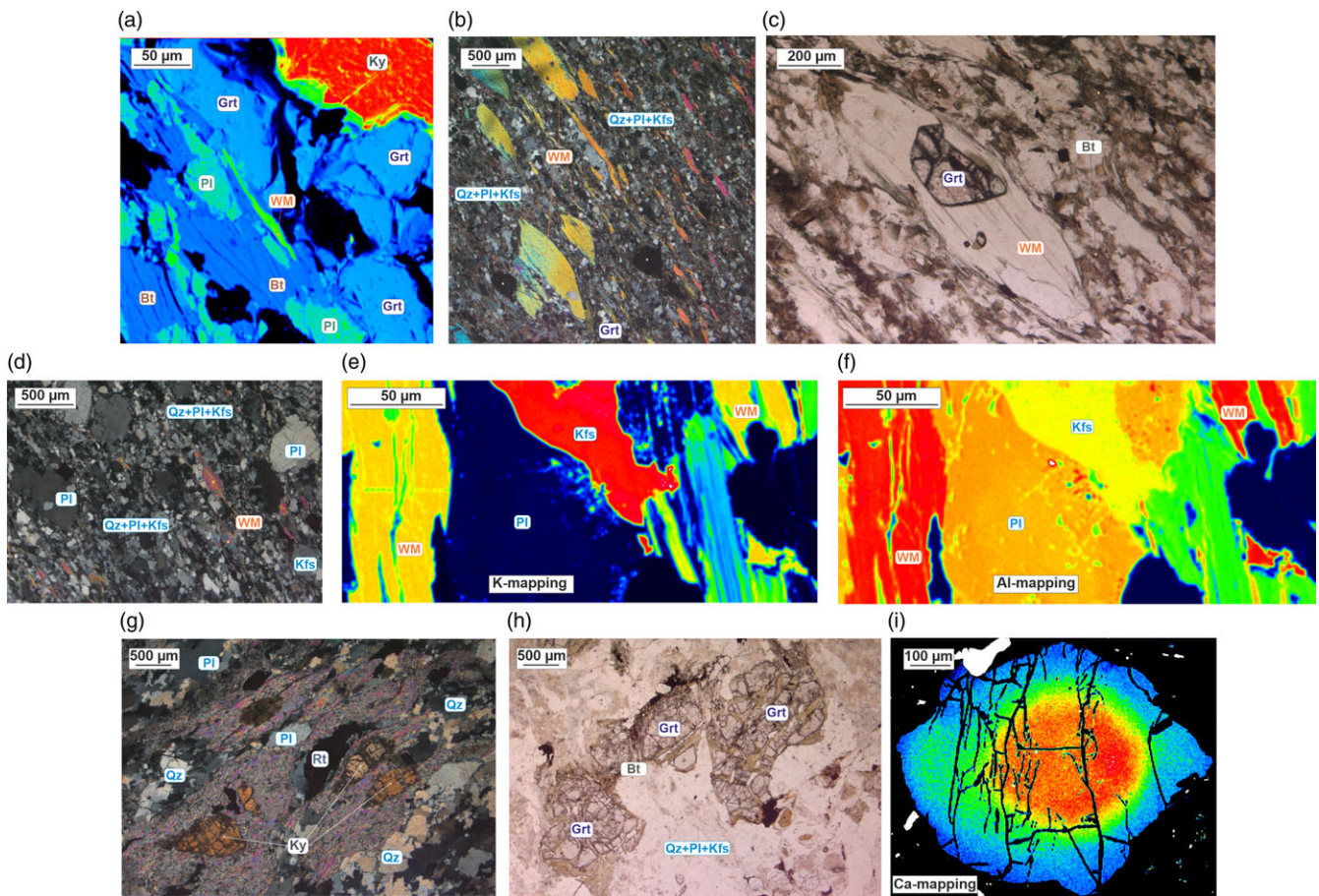


Figure 5. (Colour online) Photomicrographs and element maps of the main mineral phases and microtextures of a migmatized garnet–mica paragneiss with kyanite (garnet–mica–feldspar–quartz–kyanite melanosome AN1801/1 (a)–(c); (e), (f) and granitoid leucosome AN1801/2 (d), garnet–kyanite schist (retrograded paragneiss) AN1803 (g)–(i): (a) garnet and kyanite bounded by micas (Al element map); (b) porphyroblasts of garnet with white micas within the quartz–biotite–feldspar matrix (crossed nicols); (c) relict garnet enclosed by a coarse grain of white mica in the quartz–biotite–feldspar matrix (plane light); (d) quartz–feldspar matrix with porphyroblasts of white mica, plagioclase and K-feldspar (crossed nicols); (e), (f) association of white mica, plagioclase and K-feldspar (K and Al element maps); (g) coarse porphyroblasts of kyanite and rutile in the quartz–feldspar matrix (crossed nicols); (h) coarse porphyroblasts of garnet in the quartz–feldspar matrix (plane light); (i) zoned porphyroblast of garnet (Ca element map). Key for the abbreviations: Bt – biotite; WM – white mica; Grt – garnet; Kfs – K-feldspar; Pl – plagioclase; Qz – quartz; Rt – rutile; Ky – kyanite.

elongated, 0.5–1.5-mm-long prismatic grains (Figure 5(b), (e), (f)), whereas biotite appears as prismatic or anhedral, <0.2-mm-long grains (Figure 5(a) and (c)). White mica corresponds to phengite ($Si_{apfu} = 3.32–3.37$) or later phengite–muscovite ($Si_{apfu} = 3.01–3.15$) (Table S3) and locally encloses garnet inclusions (Figure 5(c)). In turn, leucosome granitoids are nearly free of dark-coloured minerals and exhibit gneissic textures with oriented subhedral grains of potassium feldspar and 0.05–0.8-mm-long plagioclase (albite) grains spatially associated with quartz (Figure 5(d); Table S2). Phengite ($Si_{apfu} = 3.2$) comprises varisized, unevenly distributed grains elongated in the same direction as feldspars (Figure 5(d); Table S3). Both garnet–mica paragneisses and leucosome granitoids contain numerous zircon grains, rutile and titanite.

In terms of the whole-rock composition, the garnet–mica paragneiss of the melanosome (sample AN1801/1) is characterized by significant contents of MgO (2.07 wt.%), FeO_{tot} (8.43 wt.%) and TiO_2 (1.4 wt.%) with 64.39 wt.% SiO_2 (Table 1), reflecting the existence of high modal contents of garnet and biotite in the rocks. This finding is also consistent with the notable concentrations of trace elements, such as Co, Sc and V (Table 1). In contrast, leucosome granitoids (samples AN1801/2, AN1802 and TS11100)

have low concentrations of MgO (0.08–0.76 wt.%) and FeO_{tot} (0.99–2.29 wt.%), along with high contents of $\Sigma Na_2O + K_2O$ of 6.51–8.02 wt.% and SiO_2 (73.85–78.19 wt.%), consistent with a predominance of feldspars and quartz among the main rock-forming minerals (Table 1). All the analyzed samples show differentiated REE spectra with enrichments in LREEs and depletions in HREEs and display negative Eu anomalies of ~0.6 (Figure 7), compatible with a granitoid source of their protoliths. Notably, sample AN1801/2 of the granitoid leucosome (Figure 3(d) and 7) exhibits a strongly negative Eu anomaly with $Eu/Eu^* = 0.15$, which might be indicative of a highly evolved melt and relatively earlier crystallization of plagioclase.

4.1.2. Garnet–kyanite schists (retrograded paragneisses)

These are intensively foliated coarse-grained rocks, in which 3–5-mm-long garnet porphyroblasts and 0.5–0.8-mm-long kyanite occur in the matrix (Figure 4, 5(g), (h)). Both potassium feldspar and plagioclase (albite–oligoclase) grains are preferentially oriented; mesoperthite of $Ab_{50}Or_{50}$ has also been identified (Table S2). Quartz dominates among the light-coloured minerals and forms anhedral grains (0.05–0.5 mm in size), showing irregular edges and undulating extinction

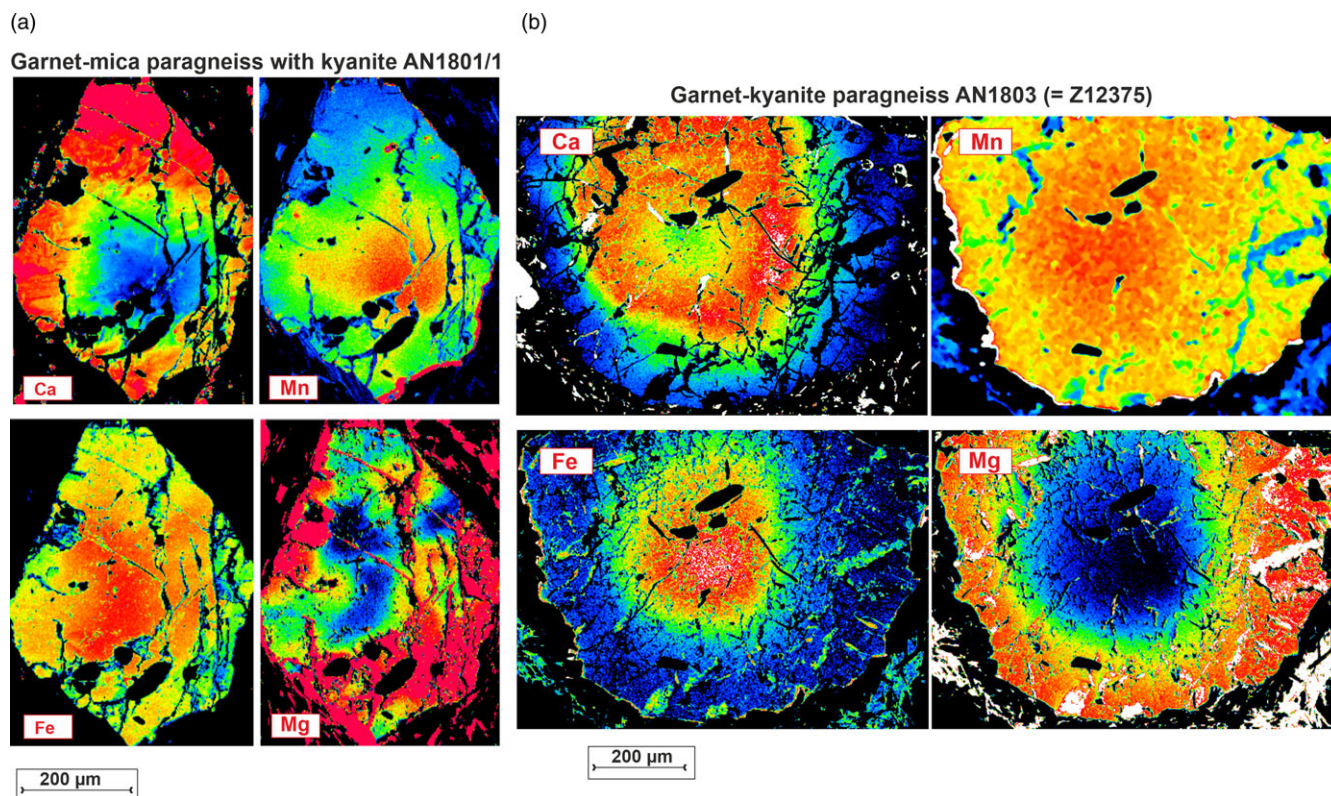


Figure 6. (Colour online) Element maps of garnets (Mn, Ca, Mg and Fe distributions) with pronounced zoning: Left: garnet–mica–feldspar–quartz–kyanite melanosome AN1801/1. Right: garnet–kyanite schist (retrograded paragneiss) Z12375 (Pilitsyna *et al.* 2019; completely analogous to sample AN1803). Consistent with Table S1.

(Figure 5(g)). Micas constitute ~15 vol.% of the rock and are largely represented by phengite–muscovite ($Si_{apfu} = 3.1$; Table S3) with minor biotite (Figure 5(h); Table S3). White mica generally forms aggregates of fine-grained flakes in the matrix, but it also locally replaces kyanite (Figure 5(g)). Coarse porphyroblasts of Fe–Mg garnet demonstrate pronounced chemical zoning (Figure 6(b)), in which near-peak and postpeak stages of garnet growth are identified. We observed smaller garnets with mostly homogenized interiors and analyzed them (Table S1). These garnets appear to have been more intensively modified by high-temperature diffusion processes, which nearly obliterated their primary growth zoning (Carlson, 2006). The only exception is calcium distribution, displaying a clear decrease from the grain cores ($X_{Ca} = 0.14$) to the rims ($X_{Ca} = 0.10$) (Figure 5(i); Table S1), reflected by a slower Ca diffusion rate compared to Fe and Mg (Vielzeuf *et al.*, 2007). Garnet–kyanite schists often include coarse grains of rutile (up to 1 mm in length; Figure 5(g)), varisized titanite, monazite and apatite with exsolution lamellae of monazite, as well as voluminous zircons.

The rocks (e.g. sample AN1803) possess SiO_2 contents of 74.79 wt.% and moderate-to-high contents of MgO and FeO_{tot} of 1.81 and 5.12 wt.%, respectively (Table 1), and demonstrate an enrichment in LREEs relative to HREEs, with a negative Eu anomaly of 0.63 (Figure 7). This finding is consistent with the element distributions obtained for the migmatized garnet–mica paragneisses. Chemical compositions and chondrite-normalized patterns of REE distribution of the studied garnet–kyanite schists are comparable to those of the granitoids, suggesting a predominance of felsic rocks in the source of their protoliths.

4.1.3. Garnet–mica schists (retrograded paragneisses) with relics of kyanite

Garnet–mica schists are the most widespread among the micaceous metasedimentary lithologies of the Koyandy complex. As described in detail in Pilitsyna *et al.* (2019), these rocks contain abundant micas (biotite and muscovite), partly resorbed garnet and plagioclase with quartz (samples AN1470, AN2201/1; Table 1). This assemblage is considered to have grown during retrogression under amphibolite facies conditions. Kyanite is only locally preserved as inclusions in garnets.

Low-grade mica schists consist of various proportions of micas and chlorite along with plagioclase and quartz (without garnet) and correspond to epidote–amphibolite facies metamorphism at the peak. However, they are juxtaposed against the high-grade paragneisses, and collectively, they all represent derivatives of terrigenous protoliths formed after erosion of granitoids, as inferred from their chemical compositions and $\epsilon_{Nd(t)}$ characteristics (Figure 7; Table 1) (Pilitsyna *et al.* 2019).

4.2. Phase equilibria modelling of the high-pressure metasedimentary rocks of the Koyandy complex

We used the Perple_X software package (version 6.9.1; Connolly, 1990, 2005) in conjunction with the internally consistent thermodynamic database of Holland & Powell (2011) to construct P–T pseudosections for the migmatized garnet–mica paragneiss with kyanite AN1801 and garnet–kyanite schist (retrograded paragneiss) AN1803 (Koyandy complex, Zheltau terrane) (Figure 8 and 9; Table 1). A P–T pseudosection was also constructed for the garnet–mica gneiss AK1904 (Aktuz complex, Chu-Kendykta terrane) sample for comparison (Figure S1; Table 1).

Table 1. Selected chemical analyses of the key rock types from the Koyandy complex (Zheltau terrane) and Aktyuz with Kemin complexes (adjacent Chu-Kendykta terrane; Skoblenko *et al.* 2023) for comparison. Major elements are in wt.%, and trace elements are in ppm. FeO(tot) = 0.9Fe2O3 + FeO; n.d. is 'not determined'; LOI is 'loss on ignition'. Chemical compositions of the gneisses of the Aktyuz complex are taken from Skoblenko *et al.* (2023); chemical compositions of samples AN1470 and AN1320 are from Pilitsyna *et al.* (2019)

	Zheltau terrane							Chu-Kendykta terrane		
	Koyandy complex							Burly Block	Aktyuz complex	Kemin complex
	Anrakhai Block									
	Garnet-mica paragneisses with kyanite				Grt-mica schist (retrograded paragneiss)	Ms-Chl schist	Garnet-kyanite schist (retrograded paragneiss)			
	melanosome	leucosome	leucosome	leucosome				Garnet-mica gneiss	Chloritized amphibole-bearing paragneiss	
AN 1801/1	AN 1801/2	TS 11100	AN 1802	AN 1470	AN 1320	AN 1803 (Z 12375)	AN 2201/1	AK 1904	AK 1913/2	
SiO ₂	64.39	78.19	74.93	73.85	71.83	77.24	74.79	70.00	69.80	72.24
TiO ₂	1.40	0.12	0.34	0.41	0.63	0.66	0.88	0.90	0.36	0.55
Al ₂ O ₃	13.30	11.61	11.80	13.56	13.16	8.97	10.10	11.07	15.96	11.46
Fe ₂ O ₃	6.61	0.98	0.73	1.66	3.57	2.25	4.91	2.19	1.63	2.33
FeO	2.48	0.10	1.63	0.78	1.02	1.25	0.70	3.60	0.60	1.52
MnO	0.12	0.01	0.07	0.03	0.07	0.06	0.10	0.09	0.10	0.11
MgO	2.07	0.08	0.76	0.67	2.11	1.74	1.81	3.89	0.80	2.26
CaO	2.34	0.39	1.90	0.57	1.36	1.48	1.33	1.57	1.94	2.35
Na ₂ O	2.45	3.17	4.11	4.69	1.39	2.08	1.05	2.32	2.93	3.29
K ₂ O	2.73	4.86	2.40	2.58	3.06	2.10	2.63	1.35	3.55	2.74
P ₂ O ₅	0.22	0.02	0.07	0.09	0.16	0.19	0.20	0.16	0.07	0.25
LOI	1.60	0.46	1.17	1.01	1.39	1.86	0.96	2.47	2.20	0.74
Total	99.72	99.99	99.91	99.91	99.76	99.86	99.46	99.60	99.94	99.83
FeOtot	8.43	0.99	2.29	2.27	4.23	3.28	5.12	5.57	2.07	3.61
Li	11.48	0.95	4.40	5.74	n.d.	n.d.	13.09	17.92	5.38	7.73
Be	1.92	2.09	0.91	1.53	1.80	n.d.	0.69	2.26	1.88	1.74
Sc	15.19	3.11	4.65	2.61	14.00	n.d.	10.66	15.30	10.78	14.95
V	139.82	6.57	20.11	26.76	78.50	56.50	101.77	95.56	5.48	36.40
Cr	74.06	10.17	1.89	16.67	82.00	56.40	78.56	66.78	19.89	65.72
Co	17.75	0.61	1.93	2.08	13.00	6.98	20.21	13.64	0.91	7.87
Ni	47.44	6.43	1.27	11.48	38.20	21.30	58.25	45.56	13.71	49.14
Cu	15.34	14.54	38.19	4.00	23.50	8.97	29.01	7.54	12.15	9.17
Zn	91.39	19.52	27.97	25.70	68.60	33.90	85.30	67.35	72.85	64.95

(Continued)

Table 1. (Continued)

Ga	16.31	12.92	11.41	13.20	18.10	8.51	13.12	14.45	16.62	14.32
Rb	79.95	110.95	55.73	63.03	140.00	59.50	77.93	52.82	67.51	66.09
Sr	126.40	22.17	138.78	155.07	135.00	95.50	115.72	113.23	102.25	238.25
Y	34.02	61.55	19.51	25.06	32.60	22.50	39.17	45.15	34.68	67.74
Zr	234.42	230.22	75.51	142.11	69.50	269.00	285.12	265.74	213.45	465.60
Nb	15.59	11.82	5.12	10.80	8.18	7.73	19.09	13.14	10.49	16.57
Mo	0.49	0.40	0.27	0.53	0.67	n.d.	1.13	0.58	0.51	0.63
Cs	2.50	0.50	0.33	0.50	5.50	0.57	0.31	1.43	1.96	0.79
Ba	603.88	515.90	714.29	572.66	601.00	282.00	714.92	214.98	1415.33	822.11
La	56.79	42.10	21.31	36.60	57.80	27.50	39.26	42.05	40.75	95.61
Ce	116.66	87.06	40.92	71.76	121.00	51.00	77.86	84.53	80.09	187.79
Pr	12.89	9.94	4.33	7.73	11.50	5.79	8.08	9.65	9.27	21.42
Nd	50.50	40.36	15.90	28.31	46.30	21.20	32.47	37.28	37.39	83.66
Sm	9.83	8.96	3.12	4.98	9.81	4.37	7.39	7.66	7.52	14.83
Eu	1.90	0.45	0.62	1.05	1.54	0.85	1.47	1.41	2.07	3.03
Gd	8.42	9.17	3.11	4.27	7.59	3.96	6.93	6.93	6.92	12.49
Tb	1.23	1.57	0.49	0.66	1.00	0.60	1.29	1.19	1.09	1.97
Dy	7.21	10.58	3.13	4.27	5.12	3.62	7.43	7.46	6.37	11.59
Ho	1.35	2.27	0.70	0.86	0.97	0.82	1.45	1.62	1.21	2.33
Er	3.82	6.87	2.51	2.61	2.34	2.36	4.05	4.36	3.39	6.94
Tm	0.52	1.02	0.43	0.39	0.43	0.33	0.61	0.67	0.52	1.06
Yb	3.57	6.84	3.36	2.74	2.47	2.40	3.77	4.28	3.41	6.79
Lu	0.52	1.00	0.59	0.42	0.34	0.32	0.53	0.64	0.54	1.03
Hf	6.27	8.52	2.38	3.86	1.91	6.79	6.98	7.13	5.50	11.78
Ta	1.21	0.35	0.37	0.76	0.70	0.65	1.52	0.96	0.59	0.78
W	1.14	0.28	0.20	0.54	1.05	1.04	1.49	1.39	0.46	0.74
Tl	0.37	0.51	0.28	0.31	n.d.	n.d.	0.32	0.21	0.31	0.33
Pb	15.30	14.66	12.18	13.46	23.00	9.06	23.63	22.48	12.48	22.34

(Continued)

Table 1. (Continued)

		Zhettau terrane				Chu-Kendyktas terrane			
		Koyandy complex				Aktyuz complex			
		Anrakhai Block				Burly Block			
		Garnet-mica paragneisses with kyanite		Grt-mica schist (retrograded paragneiss)		Garnet-kyanite schist (retrograded paragneiss)		Mica schist	
		leucosome	leucosome	leucosome	leucosome	Ms-Chl schist	Mica schist	Garnet-mica gneiss	Chloritized amphibole-bearing paragneiss
		AN 1801/1	AN 1801/2	AN 1802	AN 1470	AN 1320	AN 1803 (Z 12375)	AK 1904	AK 1913/2
melanosome	AN 1801/1	0.12	0.02	0.17	n.d.	n.d.	0.04	0.17	0.16
		22.97	15.25	7.54	21.00	11.60	15.71	19.47	15.21
		2.77	2.88	1.01	2.99	1.36	1.29	3.11	1.83
ΣREE		275.22	228.20	100.51	268.21	125.12	192.59	209.75	450.55
Eu/Eu*		0.64	0.15	0.61	0.55	0.62	0.63	0.59	0.68

Assuming that migmatization of the protolith of paragneisses occurred under suprasolidus conditions, which led to the formation of garnet-rich melanosome AN1801/1 and granitoid leucosome AN1801/2 (Figure 3), we used the reintegrated averaged whole-rock composition to constrain the approximate prograde, near-peak and retrograde stages of the metamorphic evolution of the rocks (Figure 8(a) and (b)). Garnet-kyanite gneiss sample AN1803 is a complete equivalent of sample Z12375, as considered in Pilitsyna *et al.* (2019). However, additional calculations were conducted in the present study to assess the retrograde stage evolution of the rocks by using the whole-rock compositions (Figure 9(a) and (b)).

Phase diagrams for the indicated metasedimentary rocks were constructed using the Na₂O–K₂O–CaO–TiO₂–FeO–MgO–MnO–Al₂O₃–SiO₂–H₂O model system (NKCTiFMMnASH), which was calculated assuming the saturation of an H₂O fluid (the CORK equation of state; Holland & Powell, 1998). Assuming an anatexis of metapelites, H₂O was specified as a system component consistent with loss on ignition values. The pseudosections were calculated with the solution models of Fsp(C1) for feldspars (Holland & Powell, 2003), Gt(HP) for garnet (Holland & Powell, 1998), Mica(CHA) for white mica (Coggon & Holland, 2002; Auzanneau *et al.* 2010), Bio(HP) for biotite (White *et al.* 2007) and melt(HP) for haplogranitic melt (Holland & Powell, 2001; White *et al.* 2001). Mineral assemblages of the paragneisses contain negligible contents of Fe³⁺; therefore, total iron was introduced in the calculations. Implemented whole-rock compositions are provided in mol.%, and garnet compositional isopleths are introduced into pseudosections for more accurate P–T path estimations. Garnet compositions are provided in Table S1.

4.2.1. Migmatized garnet–mica paragneiss

For sample AN1801, the wet solidus at pressures of 8–15 kbar corresponds to $T \approx 680\text{--}690^\circ\text{C}$ (Figure 8(a)), which indicates the onset of anatexis through dehydration melting of micas and water flux melting at $T > 690^\circ\text{C}$. The best reproducibility of X_{mn} , X_{ca} and X_{mg} compositional isopleths for garnet cores (Table S1) corresponds to pressures of 9–12 kbar and temperatures of 720–760°C that are interpreted as the parameters of suprasolidus garnet growth at prograde stages under increasing P–T and subsequent melting propagation conditions. The appearance of kyanite as inclusions in the marginal parts of garnet grains indicates a breakdown of white mica through the reaction of $\text{Ph} + \text{Pl} + \text{Qz} = \text{Grt} + \text{Ky} + \text{Kfs} + \text{melt}$ (Indares & Dunning, 2001) at $P > 18.5$ kbar and $T > 870^\circ\text{C}$ (Figure 8(b)). The following evolution of the rocks is related to retrograde growth of phengite–muscovite that is reflected by the intersection of X_{mn} and X_{ca} compositional isopleths of garnet rims (Table S1) and Si_{apfu} isopleths of 3.14–3.15 for phengite (Table S3) in a temperature range of 870 to 800°C at pressures of 18.5–12 kbar (Figure 8(b)). The subsequent extensive growth of biotite and muscovite associated with garnet resorption is consistent with complete melt crystallization at $P < 12$ kbar and $T < 720^\circ\text{C}$. In doing so, Zr-in-rutile thermometry yields a range of temperatures corresponding to ~650–690°C (Table S5), compatible with the near-suprasolidus conditions of the formation of rutile.

4.2.2. Garnet–kyanite schist (retrograded paragneiss)

Mineral assemblages and garnet zoning in sample AN1803 (equivalent to sample Z12375 analyzed in Pilitsyna *et al.* 2019) reflect several stages in the evolution of the rocks at prograde, near-peak, postpeak and late retrograde stages. Coarse garnet

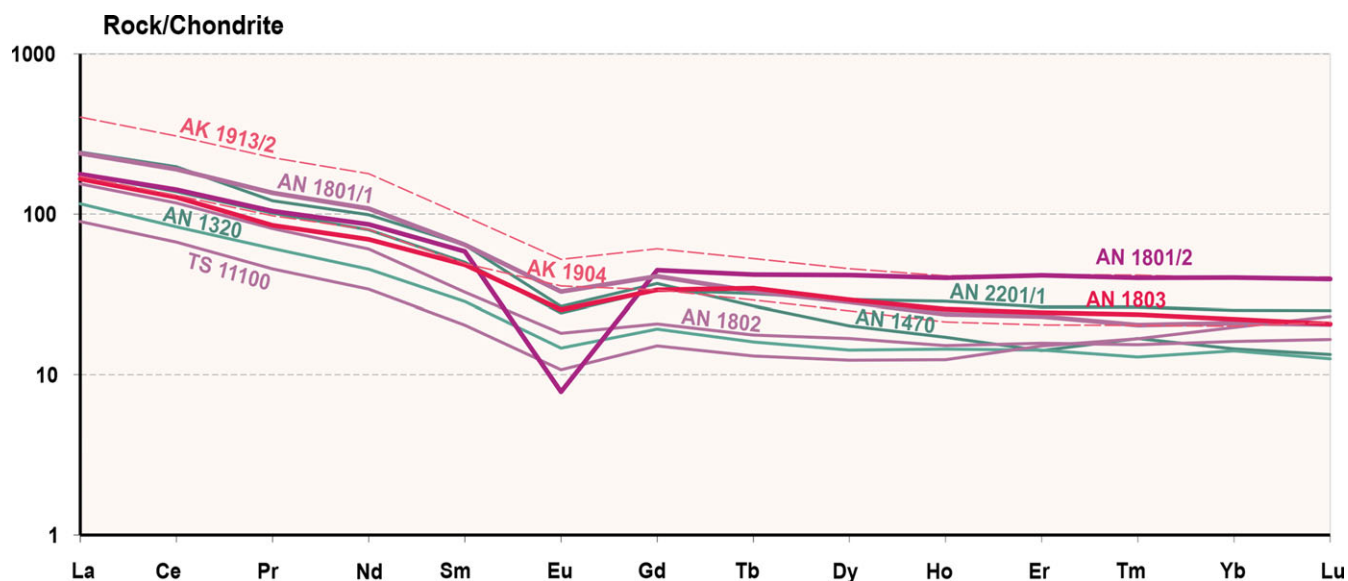


Figure 7. (Colour online) Chondrite-normalized patterns of REE distribution for metasedimentary rocks of the Zheltau and the adjacent Chu-Kendykta terranes for comparison (consistent with Table 1). Chondrite values are after Sun and McDonough (1989).

Migmatized garnet-mica paragneiss with kyanite AN1801

Reintegrated bulk composition in mol.%: SiO₂ = 76.38; TiO₂ = 0.61; Al₂O₃ = 7.86; FeO(tot) = 2.69; MgO = 1.72; MnO = 0.06; CaO = 1.48; Na₂O = 2.92; K₂O = 2.59; H₂O = 3.68

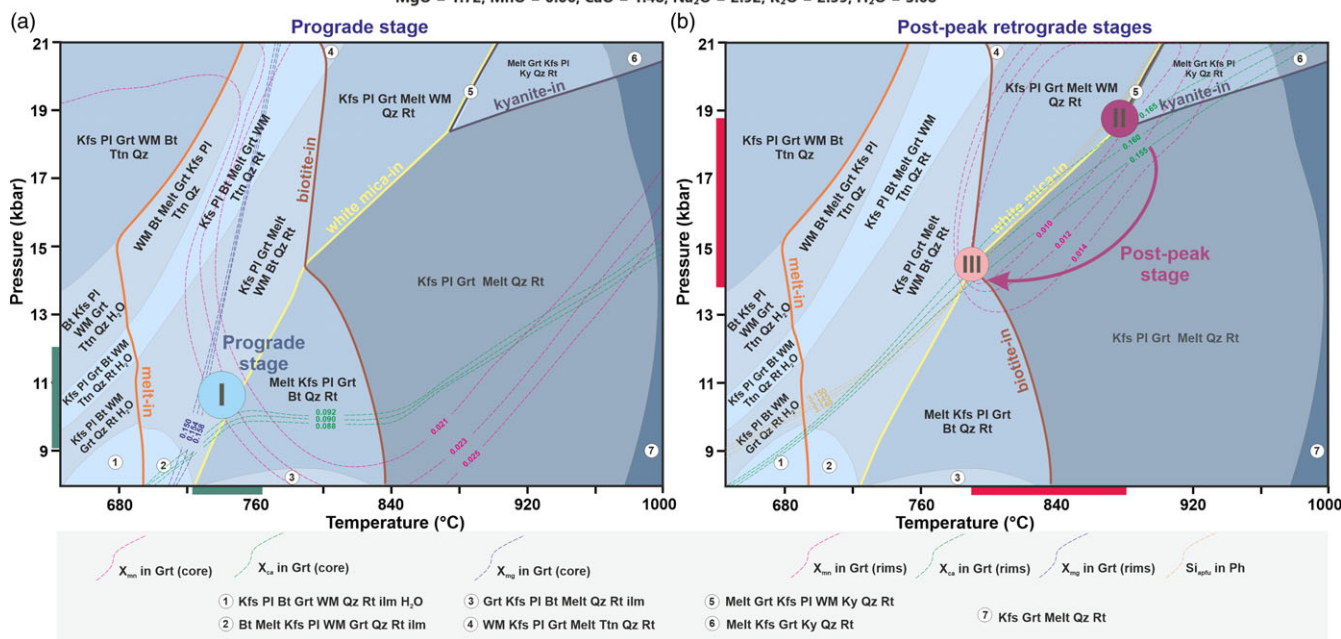


Figure 8. (Colour online) P–T pseudosections with the estimated prograde (a) and postpeak to retrograde (b) stages of metamorphism for migmatized garnet–mica paragneiss with kyanite AN1801 in the NKCTiFMnASH system, based upon the reintegrated bulk composition (given in mol.%). The details of recalculations and implemented solution models are given in Section 4.2. Coloured lines are compositional isopleths for X_{Mn} , X_{Ca} and X_{Mg} in garnet (Table S1) and Si (a.p.f.u.) in white mica (Table S3).

grains (Figure 6(b)) record prograde P–T path parameters at 8–9.5 kbar and 710–720°C (stage I) observed from the intersection of X_{Fe} , X_{Ca} and X_{Mg} isopleths (Figure 9(a); Table S1). The isopleth intersection is in the vicinity of the solidus line, which might indicate the formation of garnet cores under suprasolidus conditions. Near-peak conditions of the evolution of the rocks are defined as P = 15–17 kbar and T = 760–810°C (stage II, obtained by Pilitsyna *et al.* 2019), with the best reproducibility

of X_{Mn} , X_{Ca} , X_{Fe} and X_{Mg} compositional isopleths corresponding to mantle-inner rim parts of garnet (Figure 9(a); Table S1). The transition to the near-peak stage is determined by the disappearance of biotite to produce magnesium-rich garnet rims associated with potassium feldspar and melt via the reaction of $Bt + Ph + Pl + Qz = Grt + Kfs + melt$ (Indares & Dunning, 2001). In accordance with the phase equilibria modelling, the following temperature increase provokes phengite-dehydration melting at

Garnet-kyanite schist (retrograded paragneiss) AN 1803

Bulk composition in mol.%: SiO₂ = 79.73; TiO₂ = 0.71; Al₂O₃ = 6.34; FeO(tot) = 2.6;
MgO = 2.88; MnO = 0.09; CaO = 1.37; Na₂O = 1.09; K₂O = 1.79; H₂O = 3.41

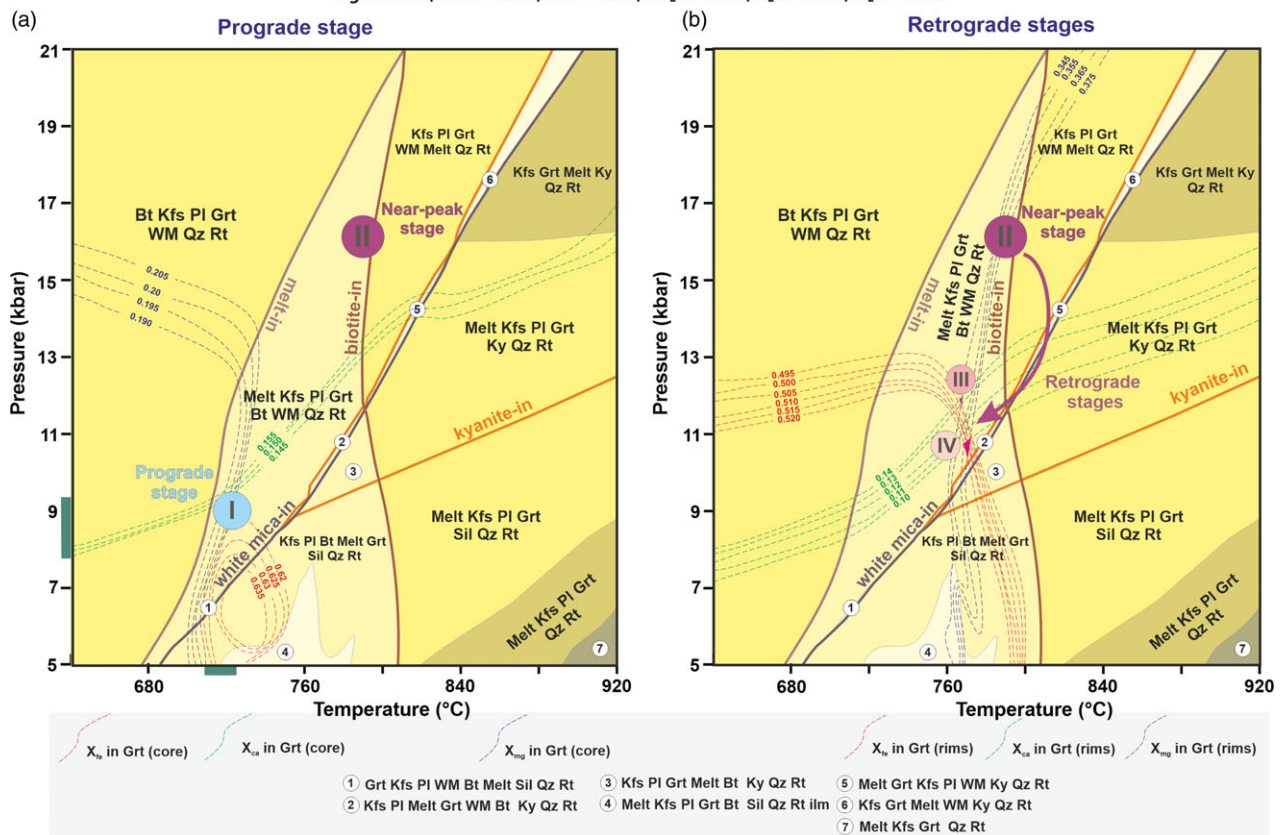


Figure 9. (Colour online) P–T pseudosections with the estimated prograde (a) and near-peak to retrograde (b) stages of metamorphism for garnet–kyanite schist (retrograded paragneiss) AN1803 in the NKCTFMnASH system based upon measured bulk compositions (given in mol.%). The details of recalculations and implemented solution models are given in Section 4.2. Coloured lines are compositional isopleths for X_{Fe} , X_{Ca} and X_{Mg} in garnet (Table S1).

$T > 800^{\circ}\text{C}$ and $P > 10$ kbar with kyanite formation (Figure 9(b)). The results of Zr-in-rutile thermometry show consistent values of $\sim 750\text{--}870^{\circ}\text{C}$ (Table S5). Finer grains of garnet (Figure 5(i)) from the same sample of garnet–kyanite paragneiss AN1803 demonstrate prominent zoning in Ca distribution with the maximum contents in the cores and a gradual decrease towards the rims, marking a decompression reaction of garnet with kyanite to produce anorthite-rich plagioclase (Ganguly & Saxena, 1984). The X_{Ca} , X_{Fe} and X_{Mg} compositional isopleths of the garnet core (Table S1) exhibit an accurate intersection in a small area of $P = 12$ kbar and $T = 770^{\circ}\text{C}$ (Figure 9(b), stage III), whereas the P–T parameters of formation of the garnet rims are constrained by the best reproducibility of X_{Ca} , X_{Fe} and X_{Mg} isopleths at $P = 10.5\text{--}11$ kbar and $T = 770\text{--}775^{\circ}\text{C}$ in the stability field of both micas (Figure 9(b), stage IV). Final melt crystallization at $T = \sim 720^{\circ}\text{C}$ is compatible with an assemblage of the common medium-grade garnet–mica paragneiss/schist, consisting of garnet, muscovite, biotite, plagioclase and quartz.

Widespread garnet–mica schists with relics of kyanite of the Koyandy complex may, therefore, represent the most altered varieties of the paragneisses, transformed to medium- to low-grade schists through a series of metamorphic events during their retrograde evolution. In turn, subordinate garnet-free schists associated with the garnet–mica schists and paragneisses (Figure 3)

evidently underwent low-grade alterations and avoided HP re-equilibration.

4.3. Geochronology and Sm–Nd isotope systematics

4.3.1. Migmatized garnet–mica paragneisses

The detrital zircon population from the granitoid leucosome of the garnet–mica migmatized paragneiss (sample AN1801/2; Figure 3(d)) exhibits euhedral and subhedral habits and well-developed oscillatory zoning and is characterized by the presence of inherited cores (Figure 10(a)). The grain sizes of these detrital zircons vary in the range of $100\text{--}200\ \mu\text{m}$, and the elongation coefficient varies from 1.5 to 2.5. The analyzed zircon cores (SHRIMP II) have Th/U ratios consistent with their magmatic origin and ranging between 0.39 and 0.69, whereas their rims demonstrate significantly lower Th/U ratios of 0.01–0.09, interpreted to have originated from HP metamorphic re-equilibration (Table 2). Furthermore, separated grains with similar Th/U ratios are also found among the studied zircons (Figure 10(a)).

The observed zircon population yielded an age range of 616–766 Ma (SHRIMP II) for their cores, with population peaks at 712 Ma, 721 Ma and 753 Ma (Figure 10(b); Table 2, 3). The core of one zircon grain revealed a Neoproterozoic crystallization age of $\sim 2556 \pm 19$

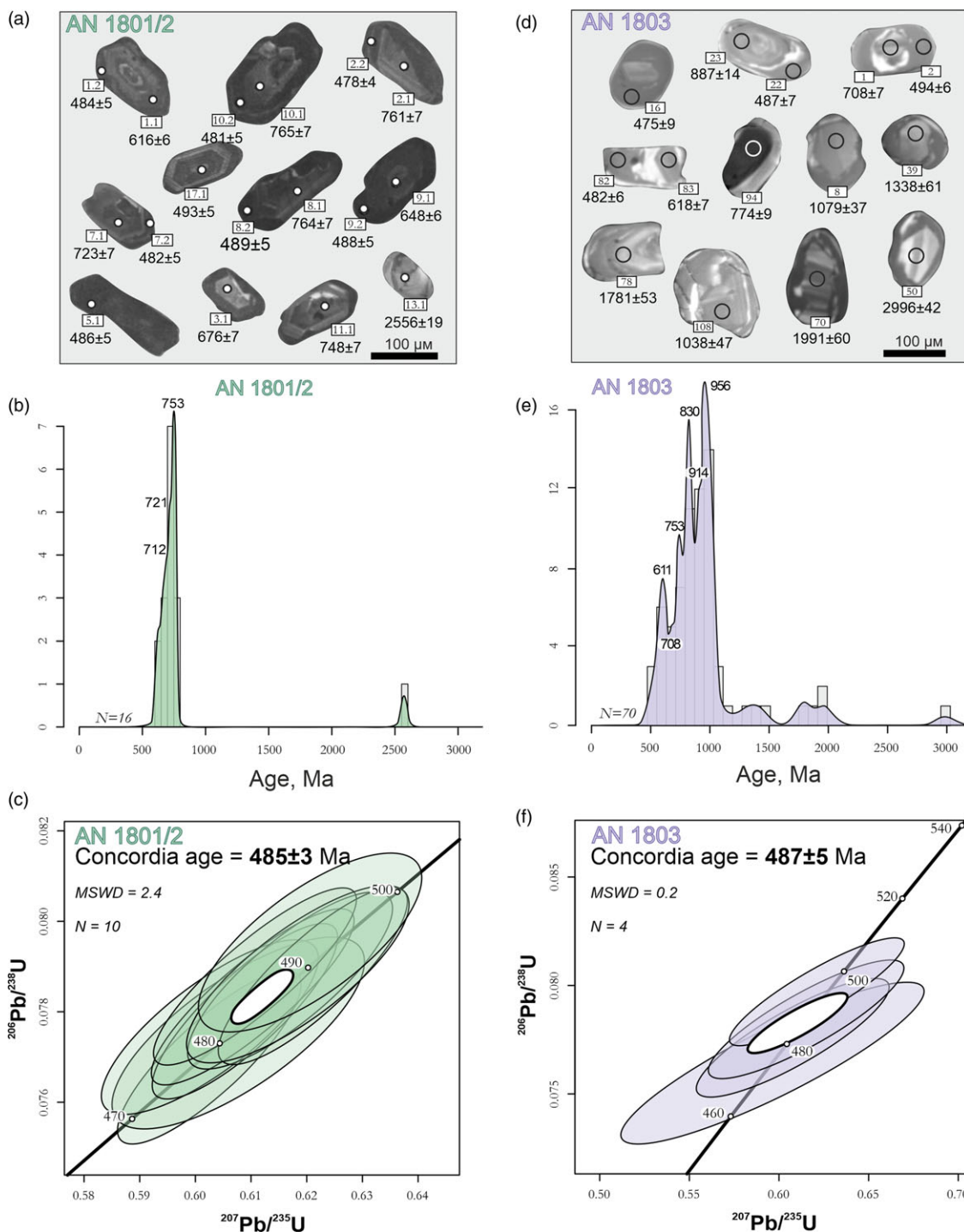


Figure 10. (Colour online) Cathodoluminescence photographs of zircon grains (a), (d), histograms of the relative probability for zircon core ages (b), (e) and concordia diagrams of younger zircon rim ages (c), (f) for paragneisses of the Koyandy complex (Zheltau terrane): (a)–(c): granitoid leucosome of garnet–mica paragneiss AN1801/2. The circles are SHRIMP II analytical spots; the numbers in the squares are in accordance with Tables 2 and 3. (d)–(f): Garnet–kyanite schist (retrograded paragneiss) AN1803. The circles are LA-ICP-MS analytical spots; the numbers in the squares are in accordance with Tables S6 and 3.

Ma, indicating the involvement of the early Precambrian basement as a source of clastic material in the protoliths of paragneisses (Table 2). The concordant $^{206}\text{Pb}/^{238}\text{U}$ age obtained from the rims of ten zircon grains and newly formed zircons corresponds to an age of 485 ± 3 Ma ($\text{MSWD} = 2.4$) (Figure 10(c); Table 2).

The garnet–mica paragneisses are characterized by negative $\epsilon_{\text{Nd}(t)}$ values of -4.9 , consistent with our inference of the derivation

of the protoliths of these rocks from a reworked, early Precambrian continental crustal source. The Nd model age $t_{\text{Nd(DM)}}$ of this source is ca. 1.6 Ga (Table 4).

4.3.2. Garnet–kyanite schists (retrograded paragneisses)

Zircon grains from the garnet–kyanite paragneiss AN1803 display subrounded habits and preserve oscillatory zoning and/or contain

Table 2. Results of ion microprobe (SHRIMP II) U–Th–Pb analyses of zircons from the granitoid leucosome of garnet–mica migmatized paragneiss AN1801/2

Spot		% ²⁰⁶ Pb _c	ppm U	ppm Th	²³² Th / ²³⁸ U	ppm ²⁰⁶ Pb*	(1) ²⁰⁶ Pb / ²³⁸ U Age	(1) ²⁰⁷ Pb / ²⁰⁶ Pb Age	% Dis- cor- dant	(1) ²³⁸ U/ ²⁰⁶ Pb*	±%	(1) ²⁰⁷ Pb* / ²⁰⁶ Pb*	±%	(1) ²⁰⁷ Pb* / ²³⁸ U	±%	(1) ²⁰⁶ Pb* / ²³⁸ U	±%	err corr	comment		
3	2.2	0.0099157	2865.6623	26.403406	0.0095202	190	478.1	4.4	482	±12	0.8800305	12.99	0.96	0.05676	0.56	0.6025	1.1	0.07699	0.96	0.8653188	zircon rim
4	10.2	0.1761864	2563.3605	19.790742	0.0079775	171	481.4	5.2	486	±23	0.8894325	12.9	1.1	0.05685	1	0.6077	1.5	0.07753	1.1	0.7325537	zircon rim
5	7.2	0.0212674	2702.157	38.33886	0.0146602	180	482.2	4.7	463	±17	-3.913825	12.88	1	0.05628	0.76	0.6026	1.3	0.07766	1	0.8003858	zircon rim
6	1.2	0.0115888	2499.5463	20.162805	0.0083349	168	484.2	4.5	476	±13	-1.59794	12.82	0.96	0.05661	0.6	0.6089	1.1	0.07801	0.96	0.8474929	zircon rim
7	5.1	0.0700074	5187.7061	61.519807	0.0122533	349	486.2	4.6	472	±13	-2.84282	12.77	0.99	0.05651	0.6	0.6103	1.2	0.07833	0.99	0.8566354	separated zircon grain
8	9.2	0.0128616	2831.4716	115.55902	0.0421701	191	488.3	4.8	486	±16	-0.408842	12.71	1	0.05686	0.73	0.617	1.2	0.07869	1	0.8133065	zircon rim
9	6.2	1.794E-29	3605.2941	31.342904	0.0089828	244	488.9	4.7	461	±13	-5.72094	12.69	1	0.05622	0.61	0.6107	1.2	0.07878	1	0.8549901	zircon rim
10	18.1	0.0059424	4632.6947	34.857035	0.0077744	314	488.9	4.6	498	±12	1.9064546	12.69	0.98	0.05717	0.56	0.6211	1.1	0.07879	0.98	0.870103	zircon rim
11	8.2	0.0422314	2551.2546	177.08831	0.0717214	173	489.1	4.8	488	±18	-0.320352	12.69	1	0.0569	0.82	0.6184	1.3	0.07883	1	0.7771923	zircon rim
12	17.1	0.0792493	1354.8844	124.26119	0.0947646	92.7	493.3	4.7	476	±20	-3.58544	12.57	0.98	0.05659	0.89	0.6206	1.3	0.07953	0.98	0.7410691	separated zircon grain
13	1.1	0.026363	1598.2661	676.92431	0.4376265	138	615.7	5.8	633	±13	2.8309975	9.977	0.98	0.06083	0.62	0.8406	1.2	0.10023	0.98	0.8448263	
14	21.1	1.2267892	1102.5228	423.99869	0.397365	97.7	625.7	6	665	±63	6.3092515	9.811	1	0.0617	3	0.868	3.1	0.1019	1	0.3196996	
15	9.1	0.1286842	1408.4278	665.22923	0.4880332	130	658.4	6.2	649	±17	-1.369645	9.299	0.99	0.06129	0.79	0.909	1.3	0.1075	0.99	0.7814188	
16	20.1	0.0150785	1258.7925	469.14889	0.3850962	119	674.3	6.4	665	±14	-1.3895	9.068	1	0.06174	0.67	0.939	1.2	0.1103	1	0.8305722	
17	3.1	0.0377952	533.26726	357.8533	0.6933823	50.7	676.3	6.8	673	±23	-0.529329	9.04	1.1	0.06196	1.1	0.945	1.5	0.1106	1.1	0.7002938	
18	4.1	0.0339776	1232.1058	607.99232	0.5098739	123	708.4	6.6	700	±16	-1.139331	8.61	0.98	0.06277	0.77	1.005	1.2	0.1161	0.98	0.7862919	
19	15.1	0	470.04407	264.99518	0.5825216	47	710.3	7.2	710	±25	-0.059932	8.584	1.1	0.06305	1.2	1.013	1.6	0.1165	1.1	0.6786911	
20	7.1	0.0034339	1012.0778	584.69161	0.596933	103	723.2	6.7	724	±15	0.043396	8.422	0.99	0.06346	0.7	1.039	1.2	0.1187	0.99	0.8152688	
21	12.1	0.9866957	399.61016	204.05675	0.5276271	41.3	724.8	7.4	702	±67	-3.177041	8.403	1.1	0.0628	3.2	1.031	3.3	0.119	1.1	0.3221903	
22	19.1	0	1280.2832	816.17148	0.6587005	135	747.5	7.1	739	±16	-1.111586	8.134	1	0.06393	0.76	1.084	1.3	0.1229	1	0.7977661	
23	11.1	0.0735967	1013.2976	574.41148	0.5857317	107	748.1	7	741	±22	-0.902664	8.126	0.99	0.06399	1.1	1.086	1.4	0.1231	0.99	0.6857427	
24	16.1	0.0254053	808.4375	418.62537	0.5350468	85.9	751.2	7.1	738	±17	-1.781641	8.091	1	0.06389	0.78	1.089	1.3	0.1236	1	0.7863852	
25	2.1	0.0193387	926.68123	551.74783	0.6152093	99.8	761.4	7.1	747	±16	-1.858816	7.976	0.99	0.06417	0.75	1.109	1.2	0.1254	0.99	0.7976953	
26	8.1	0	775.82404	399.16538	0.5316212	83.7	764.4	7.3	760	±25	-0.589028	7.943	1	0.06456	1.2	1.121	1.6	0.1259	1	0.6484903	
27	10.1	0.0217079	776.38109	382.66696	0.5092824	84.2	765.9	7.2	772	±17	0.7332509	7.926	1	0.06491	0.79	1.129	1.3	0.1262	1	0.7847909	
28	13.1	0.1327733	55.975003	233.49225	4.3101361	24	2608	34	2556	±19	-1.977803	2.006	1.6	0.1699	1.1	11.68	1.9	0.4986	1.6	0.8213627	

Errors are 1-sigma; Pb_c and Pb* indicate the common and radiogenic portions, respectively.

Error in standard calibration was 0.34% (not included in above errors but required when comparing data from different mounts).

(1) Common Pb corrected using measured ²⁰⁴Pb.

Table 3. Selected results of age peak (Gehrels, 2012) calculations for detrital zircons from the granitoid leucosome of garnet–mica migmatized paragneiss AN1801/2 and garnet–kyanite schist (retrograded paragneiss) AN1803

	MIN AGE, MA	MAX AGE, MA	PEAK AGE, MA	NUMBER OF GRAINS
AN1803	593	1443	611	5
			708	3
			753	5
			830	9
			914	10
			956	16
AN1801/ 2	662	775	712	4
			721	4
			753	6

inherited cores. Their lengths vary between 50 and 130 μm with elongation coefficients of 1.0–2.5 (Figure 10(d)). The age population (LA-ICP-MS) of the analyzed zircon grains ranges between 593 and 1443 Ma, with the main peaks at 611 Ma, 708 Ma, 753 Ma, 830 Ma, 914 Ma and 956 Ma (Figure 10(b); Table 3, Table S6). The single zircon grains yield Meso- and Palaeoproterozoic ages of 1.8–2 Ga, indicating the presence of an ancient crustal source in the protoliths of these metasedimentary rocks (Table S6; Figure 10(e); Table 3). Some of these zircons have overgrown rims, and such rims in four of the zircons yield a concordant age of 487 ± 5 Ma (MSWD=0.19) (Figure 10(f); Table S6). We interpret this age as the timing of the HP metamorphism experienced by the rocks.

A negative $\epsilon_{\text{Nd}(t)}$ value of -11.01, obtained from the garnet–kyanite retrograded paragneisses, is compatible with a source of their terrigenous protoliths through partial melting of Palaeoproterozoic crust with an Nd model age of ~ 2.2 Ga (Table 4).

5. Discussion

5.1. Precambrian tectonic affinity of the protoliths of the high-pressure paragneisses in the Koyandy complex

The observed garnet-bearing HP paragneisses of the Koyandy complex occurring in the SE part of the Anrakhai Block in the Zheltau terrane (Figure 3) have detrital zircon age distributions in the ranges of ca. 1443–593 Ma, with main peaks at 708–611 Ma, 830–753 Ma, 956–914 Ma (garnet–kyanite schist–retrograded paragneiss, sample AN1803) and ca. 766–616 Ma (granitoid leucosome of the garnet–mica migmatized paragneiss, sample AN1801/2) (Table 1–3; S6). The Sm–Nd isotope data and chemical compositions of the paragneisses with characteristic differentiated spectra of REE distributions and negative Eu anomalies of 0.63–0.64 (Figure 7; Table 4) indicate a predominance of felsic rocks in the source of the sedimentary protoliths of the paragneisses. These felsic rocks formed as a result of reworking of continental crust with an age range of ca. 2.2–1.6 Ga in accordance with their Nd model ages. The youngest single zircon grains from both types of paragneisses yielded ages of ca. 600–520 Ma, which constrain the timing of the lower limit of deposition for their protoliths as Ediacaran–lower Cambrian, whereas the upper limit is determined by the timing of HP metamorphism consistent with the obtained zircon rim ages of ca. 487–485 Ma (Figure 10(c) and (f)).

The garnet–mica schist with relics of kyanite (sample AN1470) and the low-grade muscovite–chlorite schist (sample AN1320) (Table 1) from the central part of the Anrakhai Block (Zheltau terrane) contain detrital zircon grains with peak age populations of ca. 834–667 Ma, 1051–868 Ma, 1220–1087 Ma, 1378–1296 Ma, 2539–2464 Ma and ca. 672–590 Ma, 790–695 Ma, 1332–905 Ma, 1491–1427 Ma and 2023–1991 Ma, respectively (Pilitsyna *et al.* 2019), which are similar to the age peaks of the garnet–kyanite paragneiss (sample AN1803).

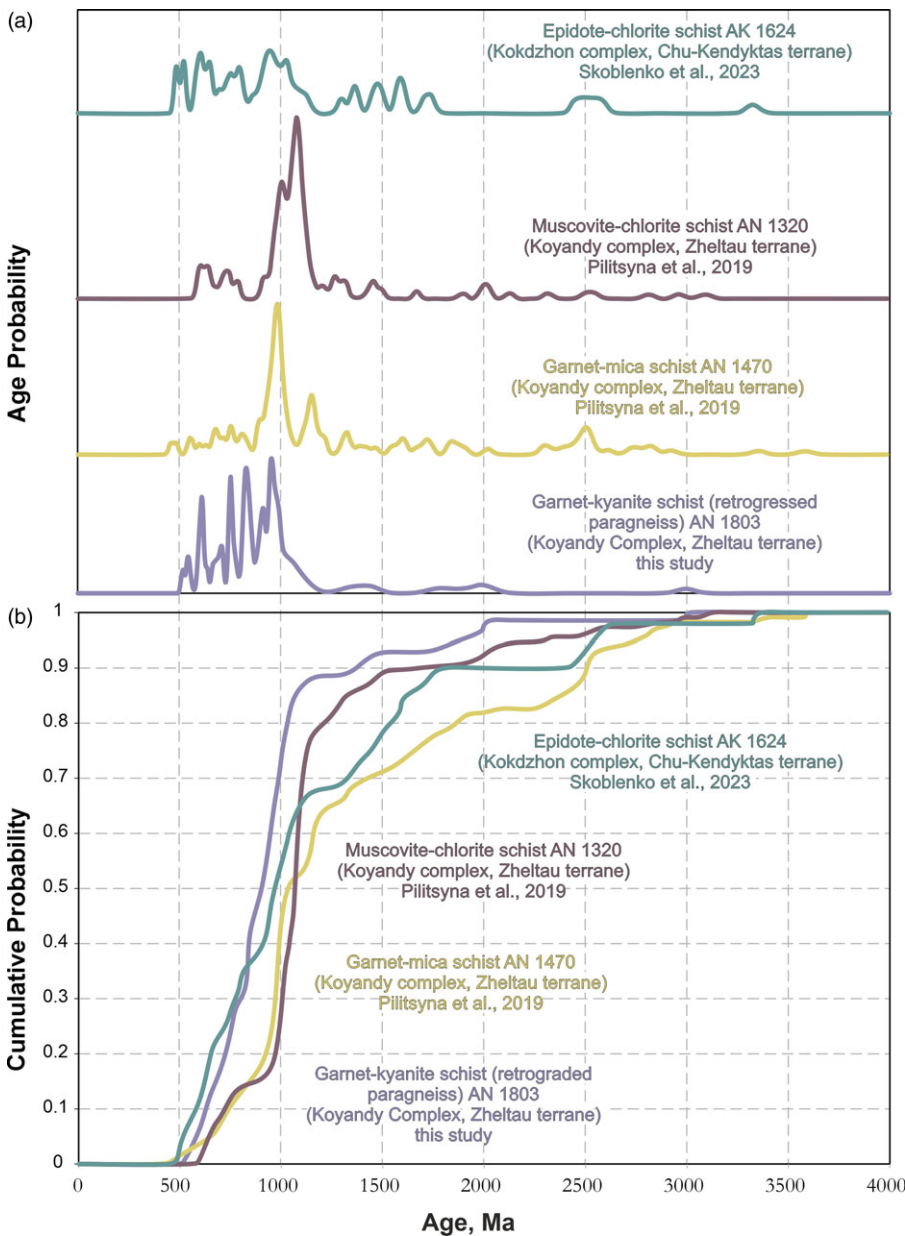
We compared the detrital zircon age peaks from the paragneisses and schists in the Koyandy complex by using ‘Overlap–Similarity’ software (Gehrels, 2000). This comparative analysis has shown a high extent of overlapping zircon age distributions between these two major metamorphic units (Figure 11; Table 5). Moreover, an epidote–chlorite schist sample (AK1624) from the adjacent Kokdzhon complex of the Chu–Kendykta terrane (Figure 1(b) and 2) exhibits detrital zircon age populations with main peaks at ca. 606 Ma, 796 Ma, 1026 Ma and 1608–1464 Ma and main spikes at 1480 and 1589 Ma (Skoblenko *et al.* 2023). Detrital zircon age assessments for samples AN1803, AN1470, AN1320 and AK1624 overlap to a degree of 0.629–0.747, and the extent of similarity is estimated to range from 0.672 to 0.758 (Table 5). These findings suggest that the protoliths of the analyzed rocks were possibly sourced from a single provenance area and that these protolith sedimentary rocks were deposited during the Ediacaran–Cambrian. On the other hand, the UHP metasedimentary rocks of the Makbal complex (Issyk–Kul terrane) are characterized by detrital zircon age distributions covering the ranges of ca. 2500–600 Ma, with the main spikes at ca. 1.95–1.75 Ga and 2.7–2.5 Ga (garnet–chloritoid–talc schists) and ca. 1.6 Ga, 1.95–1.75 Ga and 2.7–2.5 Ga (metaquartzites), which indicate much older ages of the clastic source(s) of their protoliths (Konopelko & Klemd, *et al.* 2016). We infer that an early Precambrian continental crust was the main source for the protoliths of all the indicated metasedimentary formations of the Zheltau, Chu–Kendykta and Issyk–Kul terranes in accordance with their Sm–Nd characteristics.

The zircon core ages of ca. 766–616 Ma and a single-grain age of ca. 2550 Ma obtained from the granitoid leucosome of the garnet–mica migmatized paragneiss (sample AN1801/2) in the Koyandy complex of the Zheltau terrane demonstrate distinct age peaks at 712 Ma, 721 Ma and 753 Ma. However, older zircon age estimates are virtually absent in comparison to the abovementioned garnet–kyanite paragneiss (sample AN1803). The age distribution in sample AN1801/2 implies a predominance of late Neoproterozoic (Tonian–Cryogenian) complexes in the source for the migmatized paragneisses and is uncommon for the associated metasedimentary paragneisses and schists of the Zheltau terrane, showing the main age spike at ca. 1 Ga (Figure 10(e), 11). At the same time, within the Kemin and Kokdzhon complexes of the adjacent Chu–Kendykta terrane (Figure 2), meta-arkose (sample AK1909) and amphibole-bearing paragneiss (sample AK1913/2) contain detrital zircons with cores dated at ca. 855–574 Ma and ca. 831–518 Ma, respectively (Skoblenko *et al.* 2023). We correlated the detrital zircon age assessments of samples AN1801/2, AK1909 and AK1913/2 by using ‘Overlap–Similarity’ software (Gehrels, 2012). The rocks share many similarities in terms of the statistics of their zircon age peaks (Figure 12) and show a degree of overlap in the age data, varying from 0.510 to 0.754, i.e. proposing a possible single provenance area for the protoliths of these rocks (Table 6).

Hence, we posit that protoliths of the studied paragneisses and schists appear to have contained the same sedimentary cover as the

Table 4. Sm–Nd isotope data for the studied paragneisses within the Koyandy complex (Zheltau terrane)

Sample	Concentrations, µg/g		Isotopic ratios			Best age, Ma	T _(DM) , Ma	ε _{Nd} (T)
	Sm	Nd	¹⁴⁷ Sm/ ¹⁴⁴ Nd	¹⁴³ Nd/ ¹⁴⁴ Nd	±			
Garnet-kyanite schist (retrograded paragneiss) AN1803	8.01	39	0.1242	0.5118	0.000020	500	2241	–11.01
Granitoid leucosome of the garnet-mica paragneiss AN1801/2	9.68	44.25	0.1331	0.5122	0.000006	500	1597	–4.94

**Figure 11.** (Colour online) Normalized (a) and cumulative (b) probability plots (Gehrels, 2012) with the age distributions obtained for detrital zircons from garnet-kyanite schist (retrograded paragneiss) AN1803 (this study), muscovite-chlorite schist AN1320 and garnet-mica schist AN1470 (Pilitsyna *et al.* 2019) from the Koyandy complex (Zheltau terrane), and epidote-chlorite schist AK1624 of the Kokdzhon complex (Chu-Kendykta terrane; Skoblenko *et al.* 2023). Consistent with Table 5.

Zheltau and Chu-Kendykta terranes, whereas Palaeo-, Meso- and Neo-Proterozoic metamorphosed felsic volcanic rocks and granitoids constituted the basement of these terranes. The obtained zircon core age ranges and the Sm–Nd characteristics of the

analyzed paragneisses and their derivatives are believed to reflect the long-term evolution of their protoliths prior to the onset of early Palaeozoic HP metamorphism. This metamorphic event and the associated deformation encompassed multiple stages of

Table 5. Comparison of the U–Th–Pb zircon data for the studied garnet–kyanite schist (retrograded paragneiss) AN1803 (this study), muscovite–chlorite schist AN1320 and garnet–mica schist AN1470 (Pilitsyna *et al.* 2019) from the Koyandy complex (Zheltau terrane) and epidote–chlorite schist AK1624 of the Kokdzhon complex (Chu–Kendykta terrane; Skoblenko *et al.* 2023). The degree of overlap determines whether two curves contain overlapping ages, and the degree of similarity displays whether overlapping ages have similar proportions. A value of 1.0 indicates a perfect match of all grains derived from the same source; 0.0 reflects no age match (Gehrels, 2000)

OVERLAP				
AN 1803				
AN 1470	0.689	AN 1470		
AN 1320	0.747	0.699	AN 1320	
AK 1624	0.669	0.735	0.629	AK 1624
SIMILARITY				
AN 1803				
AN 1470	0.728	AN 1470		
AN 1320	0.689	0.712	AN 1320	
AK 1624	0.748	0.758	0.672	AK 1624

continental crustal growth, its subsequent metamorphic transformation, uplift and erosion of all crustal complexes and transport and deposition of all detrital material.

Manifestations of granitoid magmatism at ~2.3 Ga and ~1.8 Ga have been reported from the Kuilyu complex of the Middle Tien Shan (Naryn–Sarydzhas) terrane (Kröner *et al.* 2017b), as well as from the Zheltau terrane (Pilitsyna *et al.* 2019) and the northern part of the Tarim Craton (He *et al.* 2013) (Figure 1(b)). Magmatic rock assemblages of ~1.6 Ga are unknown within our study area; however, this age window is recorded by quartzites or quartzite–schist sequences of the Akbastau and Makbal Formations in the adjacent Chu–Kendykta and Issyk–Kul terranes (Figure 1(b)) and marks the youngest magmatic episode providing the 1672–1625 Ma zircons (Kanygina *et al.* 2019; Alexeiev *et al.* 2020). The age range of 1.5–1.3 Ga is traced within the Chinese Central Tien Shan terrane and the Yili Block at ca. 1450–1410 Ma and ca. 1329 Ma (Huang *et al.* 2019; He *et al.* 2015), the Issyk–Kul terrane at ca. 1.3 Ga (Kröner *et al.* 2013) and the Ulutau terrane at ca. 1338 Ma (Tretyakov *et al.* 2022) (Figure 1(b)). A pronounced age peak at ca. 1.1–0.9 Ga, observed from the studied paragneisses and schists, correlates well with the episodes of granitoid magmatism within the Issyk–Kul and Kokchetav terranes at ca. 1.1 Ga (Degtyarev *et al.* 2011; Tretyakov *et al.* 2011a, b; Kröner *et al.* 2013; Kushnareva *et al.* 2022) and the Aktau–Yili terrane at ca. 925 Ma (Tretyakov *et al.* 2015; Alexeiev *et al.* 2021) (Figure 1(b)). Finally, the late Tonian age range of 840–770 Ma is widespread within the Zheltau and adjacent Chu–Kendykta terranes and documents the timing of voluminous granitoid magmatism in the North Tien Shan and South Kazakhstan (Kröner *et al.* 2012; Pilitsyna *et al.* 2019; Tretyakov *et al.* 2019; Skoblenko *et al.* 2022, 2023). The youngest zircon age peaks of ca. 700–600 Ma are assigned to a major part of the early Palaeozoic metasedimentary rocks of the Zheltau and Chu–Kendykta terranes (Skoblenko *et al.* 2022, 2023; this study); however, their source is unknown within the observed area because it might be either located beyond the study region or unexposed.

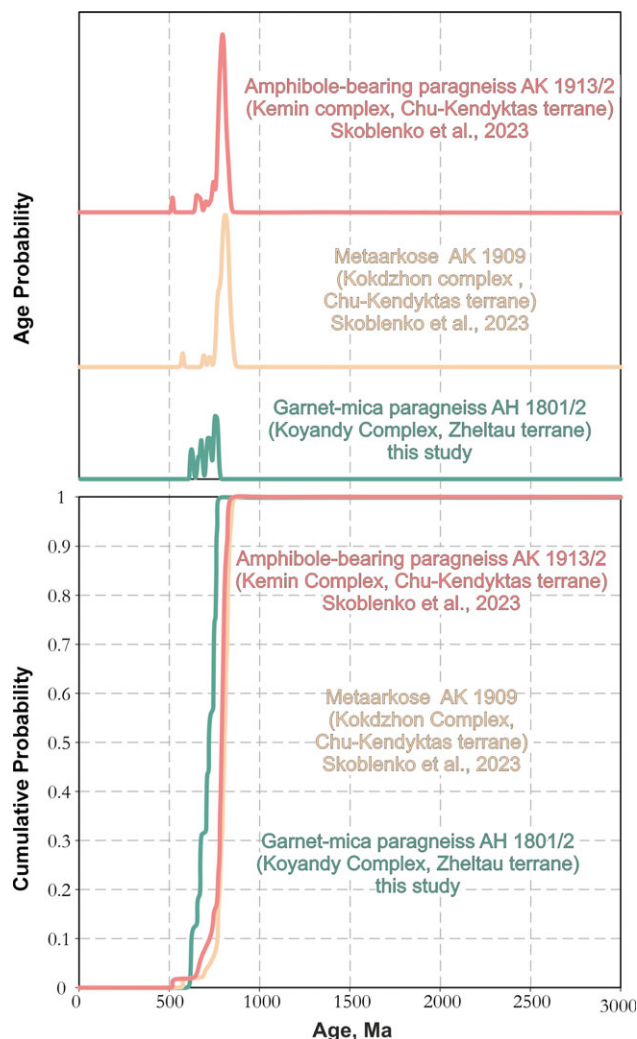


Figure 12. (Colour online) Normalized (a) and cumulative (b) probability plots (Gehrels, 2012) with the age distributions obtained for detrital zircons from the migmatized garnet–mica paragneiss (leucosome) AH1801/2 of the Koyandy complex (Zheltau terrane; this study), meta-arkose AK1909 of the Kokdzhon complex and amphibole-bearing paragneiss AK1913/2 of the Kemin complex (Chu–Kendykta terrane; Skoblenko *et al.* 2023). Consistent with Table 6.

5.2. High-pressure metamorphism of continental crust within the Zheltau and adjacent terranes of the SW part of the Central Asian Orogenic Belt in the late Cambrian–Early Ordovician

Multiple lines of evidence for the occurrence of UHP metamorphism between 530 and 470 Ma have been reported for the Kokchetav, Issyk–Kul, Chu–Kendykta and Zheltau terranes within the western segment of the CAO (e.g. Shatsky *et al.* 1999; Togonbaeva *et al.* 2009; Ragozin *et al.* 2009; Alexeiev *et al.* 2011; Rojas–Agramonte *et al.* 2013; Klemd *et al.* 2014; Meyer *et al.* 2014; Konopelko *et al.* 2012; Konopelko & Klemd, 2016; review of Skoblenko & Degtyarev, 2021) (Figure 1(b)). Formation of the early Palaeozoic UHP rocks is believed to have been related to the subduction of different rock associations to depths of at least 60 km and possibly deeper to the stability field of coesite (Makbal complex, Issyk–Kul terrane; Zerendy Group; Kokchetav terrane) or even of diamond (Zerendy Group; Kokchetav terrane). The age estimates, which correspond to the near-peak stages of UHP

Table 6. Comparison of the U–Th–Pb zircon data for the studied migmatized garnet–mica paragneiss (leucosome) AH1801/2 of the Koyandy complex (Zheltau terrane; this study), meta-arkose AK1909 of the Kokdzhon complex and amphibole-bearing paragneiss AK1913/2 of the Kemin complex (Chu–Kendykta terrane; Skoblenko *et al.* 2023). The degree of overlap determines whether two curves contain overlapping ages, and the degree of similarity displays whether overlapping ages have similar proportions. A value of 1.0 indicates a perfect match of all grains derived from the same source; 0.0 reflects no age match (Gehrels, 2000)

OVERLAP			
AH1801/2			
AK1909	0.510	AK1909	
AK1913/2	0.658	0.754	AK1913/2

metamorphism, were mostly obtained for eclogites by using U–Pb zircon and Sm–Nd with Lu–Hf garnet isochron dating. Although eclogites tend to show better preservation of HP mineral parageneses, deciphering the geochemical affiliation of eclogites and reconstructing the palaeotectonic position of their protoliths are challenging tasks. Accordingly, interpretations of oceanic ridge versus intraplate continental magmatism have been suggested by different authors for the eclogites of the Makbal (Meyer *et al.* 2014 vs. Rojas-Agramonte *et al.* 2013) and Aktyuz (Rojas-Agramonte *et al.* 2013 vs. Klemd *et al.* 2014) complexes of the Issyk-Kul and Chu–Kendykta terranes, respectively. Similarly, Precambrian pelitic sedimentary sequences (Konopelko & Klemd, 2016) versus hydrothermally altered oceanic crust (Meyer *et al.* 2014) are proposed as the protoliths for the UHP garnet–talc–chloritoid schists of the Makbal complex (Issyk-Kul terrane). Moreover, the origin of early Palaeozoic UHP metamorphism within the western CAOB is interpreted to have been closely related to the subduction of various fragments of continental crust under eclogite-facies conditions. This interpretation is supported by the findings of the involvement of Precambrian continental crust in subduction processes regarding the evolutionary history of the Zerendy Group of the Kokchetav terrane in Northern Kazakhstan (Claoue-Long *et al.* 1991). Zircons recovered from diamondiferous garnet–biotite gneisses in the Zerendy Group have yielded U–Pb ages of UHP metamorphism at ca. 530 Ma, compatible with the ages obtained from the spatially associated eclogites (Shatsky *et al.* 1993).

In the SW part of the CAOB in the North Tien Shan, coesite-bearing garnet quartzites of the Makbal complex (Issyk-Kul terrane) are known as strongly metamorphosed terrigenous crustal formations. However, zircon ages obtained from these rocks have not provided any constraints for the timing of UHP metamorphism; rather, the obtained data provided ages for their protoliths (Konopelko & Klemd *et al.* 2016). Two age clusters of ~509–498 Ma (U–Pb zircon dating) and ~470 Ma (Lu–Hf garnet isochron dating), which are thought to be consistent with the near-peak stage of metamorphism, were obtained from the amphibolised eclogites of the Makbal complex (Issyk-Kul terrane) (Konopelko *et al.* 2012; Rojas-Agramonte *et al.* 2013). Diverse age assessments of the near-peak stage of UHP re-equilibration of ca. 502 Ma (U–Pb dating of zircon rims) and ca. 475 Ma (Sm–Nd garnet isochron dating) were also obtained for the associated garnet–talc–chloritoid schists (Konopelko *et al.* 2012; Meyer *et al.* 2014). Protoliths of the UHP rocks of the Makbal complex were, hence, considered to have been subducted under the Chu–Kendykta (North Tien Shan) terrane during the closure of the Kara-Archa

ocean basin (Konopelko *et al.* 2012) and then subjected to metamorphic transformations during the time window of 509–470 Ma. These multiple deformed and metamorphosed rock associations were subsequently exhumed as tectonic slivers, consisting of metamorphosed continental crustal assemblages intercalated with derivatives of ancient oceanic lithosphere, recorded by the ages of inherited zircon cores and Sm–Nd with Lu–Hf isotope data.

Metamorphic complexes of the Zheltau (South Kazakhstan) and Chu–Kendykta terranes (North Tien Shan) bear a strong resemblance in terms of the development of their Precambrian meta-magmatic and metasedimentary formations, which show strong similarities in the ages and compositions of their protolith source (Paragraph 5.1; Skoblenko *et al.* 2022). The HP rocks attributed to the Koyandy (Zheltau terrane) and Aktyuz complexes (Chu–Kendykta terrane) are located at a distance of ~100 km relative to each other (Figure 2) and are separated by an early Palaeozoic (531–520 Ma based on plutonic units) Dzhalaïr–Naiman ophiolite zone (Ryazantsev *et al.* 2009; Kröner *et al.* 2012). The metamorphic history of the high-grade rocks of both complexes is, therefore, expected to have involved the same tectonic events associated with the evolution of the Dzhalaïr–Naiman ocean basin.

Variably amphibolised eclogites and garnet pyroxenites (only the Koyandy complex) that are spatially associated with HP garnet-bearing gneisses and their retrograded derivatives within the Koyandy and Aktyuz complexes are juxtaposed against moderate- to low-grade gneissic granites, schists and locally occurring marbles. None of these rocks shows any mineralogical or textural evidence for HP re-equilibration. Zircons from garnet pyroxenites of the Koyandy complex yield a mean U–Pb age of HP metamorphism of ca. 490 Ma (Alexeiev *et al.* 2011) at P–T conditions of 15–19 kbar and 750–850°C (Pilitsyna *et al.* 2018a). A Lu–Hf garnet isochron age (~474 Ma) has been interpreted as the near-peak stage, HP metamorphism of the eclogites in the Aktyuz complex at P = 21 kbar and T = 670°C (Rojas-Agramonte *et al.* 2013). In turn, zircons from the HP garnet gneisses in the Aktyuz complex, which contains eclogite bodies of variable sizes, display two age clusters of ca. 844 Ma (zircon cores) and ca. 490 Ma (zircon rims and separated grains). These ages mark two main stages of the evolution of the host rocks in the late Neoproterozoic (emplacement of their protoliths) and in the latest Cambrian (HP metamorphism of the gneisses' protoliths) and the following stages of rock exhumation at 490–471 Ma (Skoblenko *et al.* 2023).

An affinity of the garnet-bearing gneisses to the HP rocks formed at P = ~13–15 kbar and T = 635–745°C has been suggested previously by Orozbaev *et al.* (2010). This comparison is in agreement with the preliminary results of pseudosection modelling in conjunction with the garnet isopleth geothermobarometers of P = 10 kbar and T = 700°C at the prograde stage of garnet nucleation and P = 14 kbar and T = 760°C at the near-peak stage of the formation and melting propagation of garnet rims (Figure S1; Table S1). Garnet–mica and garnet–kyanite paragneisses of the Koyandy complex formed at the prograde metamorphic stage at P = 9–12 kbar and T = 720–760°C, whereas the near-peak to retrograde stage of development occurred at P = 15–18 kbar and T = 750–870°C (Pilitsyna *et al.* 2019; this study (Figure 8 and 9)). Detrital zircons obtained from the paragneisses and schists show different age distributions in the cores (Paragraph 5.1), whereas the rims appear to have grown during HP re-equilibration at ~487–485 Ma. This age range is compatible with the age estimate of ca. 490 Ma known from the eclogite-bearing garnet gneisses of the Aktyuz complex (Figure 13).

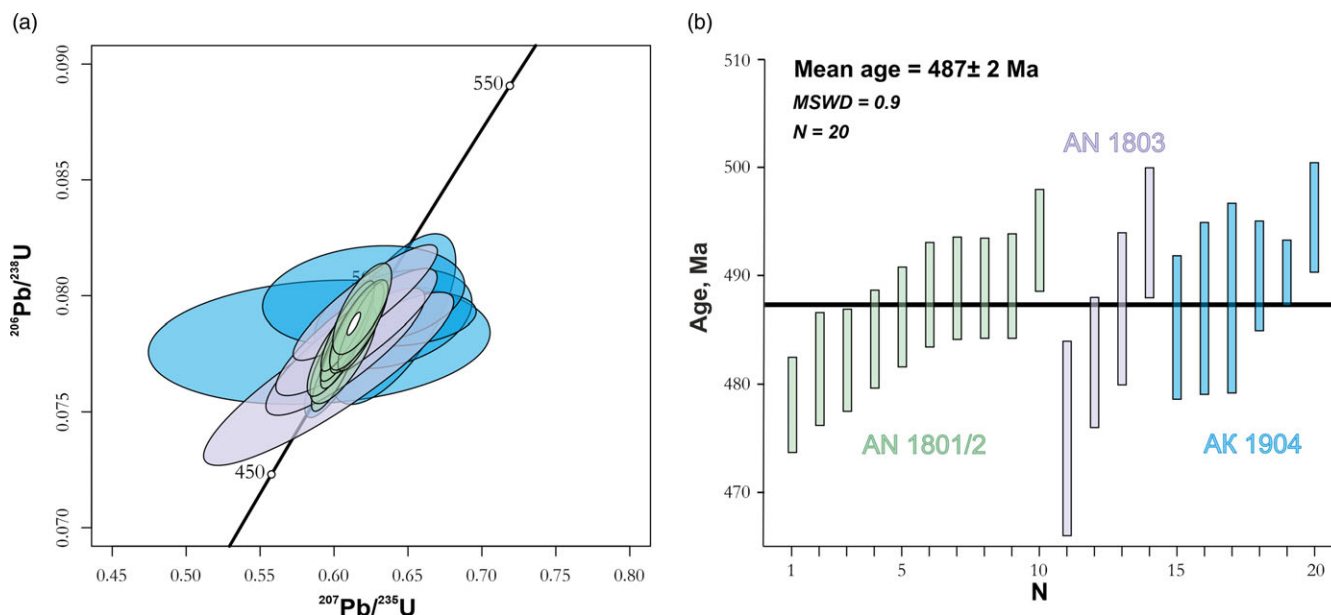


Figure 13. (Colour online) Concordia diagram and normalized probability plot (Gehrels, 2012) for zircon rim ages corresponding to the timing of the high-pressure (HP) metamorphism re-equilibration from the garnet–kyanite schist (retrograded paragneiss) AN1803 (Koyandy complex, Zheltau terrane; this study), granitoid leucosome of garnet–mica paragneiss AN1801/2 (Koyandy complex, Zheltau terrane; this study) and garnet–mica gneiss AK1904 (Aktuz complex, Chu-Kendykta terrane; Skoblenko *et al.* 2023).

Thus, we propose a clockwise, ‘subduction-type’ P–T evolution trajectory for all the early Palaeozoic UHP metamorphic rocks of the Makbal, Aktuz and Koyandy complexes in the SW part of the CAO (Figure 1(b)). The zircon age estimates obtained from the HP quartz–feldspar gneisses and their retrograded varieties indicate the involvement of crustal rocks in a Precambrian basement (Aktuz complex; magmatic zircon cores of Tonian age) and the Ediacaran–Cambrian sedimentary cover of this basement (Makbal, Kemin and Koyandy complexes; detrital zircons) in subduction zone processes during the closure of the Palaeo-Asian Ocean in the latest Cambrian through Early Ordovician.

5.3. Assessment of the existing models of the Cambrian–Early Ordovician evolution of metamorphic complexes in the Zheltau and adjacent terranes in the SW part of the Central Asian Orogenic Belt

Based on the results of our study and the extant data in the literature, we propose a tectonic model explaining the geological evolution of the Precambrian metamorphic complexes in the Zheltau and Chu-Kendykta terranes within the SW segment of the CAO (Skoblenko *et al.* 2022; this study). We recognize that the Precambrian evolutionary trend of the Issyk-Kul terrane differs from that of the Zheltau and Chu-Kendykta terranes (Degtyarev *et al.* 2017; Kanygina *et al.* 2021). The Ediacaran–Cambrian continental rifting and seafloor spreading processes resulted in the opening of the Palaeo-Asian Ocean, encompassing multiple seaways that separated various continental blocks. The remnants of one of these seaways occur in the Cambrian Dzhalaïr–Naiman zone (Figure 2) and consist of variously serpentinized mafic–ultramafic rocks of residual and layered complexes, gabbroids and plagiogranites, as well as bimodal basalt–rhyolite series (Ryazantsev *et al.* 2009). Metagabbroids in the Dzhalaïr–Naiman zone are ~531 Ma in age and are part of the Kopurelisay complex within the Aktuz continental block (Chu-Kendykta terrane). Serpentinites and gabbroids in the Anrakhai

block within the Zheltau terrane (Figure 2 and 3) may potentially be part of the Dzhalaïr–Naiman zone, and together with the Kopurelisay complex, they may represent a suprasubduction-zone (SSZ) ophiolite. This SSZ oceanic crust evolved into the development of an enigmatic island arc (Sulusay island arc associated with OIB volcanism) at ~510–500 Ma (Ryazantsev *et al.* 2009; Degtyarev, pers. comm.), reminiscent of island arc-type ophiolites (Dilek & Furnes, 2011, 2014). Metamorphic formations containing HP mineral assemblages (i.e. Koyandy and Aktuz complexes) within the studied terranes of South Kazakhstan and the North Tien Shan generally occur with tectonically juxtaposed fragments of ophiolites (Figure 2 and 3).

The presence of eclogites in both the Koyandy and Aktuz complexes of the Zheltau and Chu-Kendykta terranes is a distinguishing geological feature (Paragraph 5.2). However, the available different ages of HP metamorphism (~490 and ~474 Ma) and variable modal and chemical compositions of the metamorphic and ophiolitic rock units have allowed different interpretations for the Cambrian–Early Ordovician tectonic evolution of those eclogites. Alexeiev *et al.* (2011) and Kröner *et al.* (2012) suggested, for example, that NE subduction of the oceanic lithosphere of the Dzhalaïr–Naiman basin under the Zheltau terrane might have involved subduction erosion, i.e. rock material scraped off from the bottom of the Zheltau terrane in the upper plate and downwards transport of this eroded material along the subduction interface at approximately 490–485 Ma. During this subduction process, the eroded crustal fragments underwent metamorphic transformations up to eclogite-facies conditions, recorded by the U–Pb zircon age of garnet pyroxenites intercalated with eclogites of ca. 490 Ma (Koyandy complex). Continued subduction of the oceanic lithosphere led to the terminal closure of the Dzhalaïr–Naiman basin and the collision of the Zheltau and Chu-Kendykta terranes at approximately 485–474 Ma. Partial subduction of the passive margin of the Chu-Kendykta terrane caused HP metamorphism of its siliciclastic and carbonate rock assemblages in the latest Cambrian, followed by their exhumation

(e.g. as considered in models of Dilek *et al.* (2012); Barbero *et al.* (2023)). The second stage subduction of oceanic lithosphere is marked by a Lu–Hf garnet isochron age (ca. 474 Ma) of the eclogites in the Aktyuz complex, which were similarly exhumed along with the adjacent crustal formations after slab break-off.

On the other hand, Pilitsyna *et al.* (2018b) proposed that two different oceanic basins must have existed in the vicinity of the Zheltau and Chu-Kendykta terranes during the Cambrian; the terranes were separated by the Dzhalaïr-Naiman ocean basin that existed between the Zheltau and Chu-Kendykta terranes, while another basin existed to the north of the Zheltau terrane. Diachronous processes of subduction of the ocean floor within these two basins during 500–474 Ma led to the partial subduction of the passive margin of the Zheltau terrane under the Aktau-Yili (?) terrane (Figure 1(b)) to form eclogites and garnet pyroxenites (aged ca. 490 Ma), which are currently spatially associated with the HP felsic gneisses and symplectite-bearing peridotites and with the partial subduction of the continental margin of the Chu-Kendykta terrane under the Zheltau terrane after the closure of the Dzhalaïr-Naiman basin. This event resulted in the formation of eclogites and quartz–felspar rock assemblages at approximately 474 Ma. Exhumation of all the HP complexes occurred during the Early Ordovician.

We evaluated the contradicting aspects of these two models based on our new data obtained for the Zheltau and Chu-Kendykta terranes. Age clusters of ~844 Ma and ~490 Ma obtained from the zircons recovered from the high-grade garnet gneisses of the Aktyuz complex (Skoblenko *et al.* 2023), which are spatially associated with the 474 Ma eclogites, provide strong geological and geochronological evidence for the partial subduction of the continental crust of the Chu-Kendykta terrane during the latest Cambrian. This association makes the origin and affinity of the eclogites in the Aktyuz complex ambiguous. Moreover, even assuming a diachronous prograde-to-peak metamorphism of the continental crust (gneisses) and oceanic (?) (eclogite) complexes of the Chu-Kendykta terrane and their mutual exhumation at 490–471 Ma reflected by zircon rim ages, it appears to be hardly feasible for the gneisses to have retained garnet zoning during ~20–15 Ma of residence until the protoliths of eclogites achieved HP conditions. In fact, both eclogites and enclosing garnet gneisses of the Aktyuz complex exhibit well-developed textural evidence of ‘prograde-type’ zoning with a decrease in Mn contents from cores to rims (Figure S2; Table S1). In turn, the spatial closeness of the Zheltau and Chu-Kendykta terranes, nearly equal compositions of the ophiolitic complexes developed in the NE part of the Anrakhai block (Figure 3) and within the Kopurelisay complex (Figure 2), along with the obtained age of HP metamorphism of garnet gneisses of the Aktyuz complex compatible to that of the eclogites with garnet pyroxenites of the Koyandy complex and garnet–mica paragneisses of ca. 490–487 Ma, lend support for a single ocean basin (i.e. Dzhalaïr-Naiman basin) evolution of the studied complexes, rather than two different basins. Notably, despite very similar characteristics of the high-grade crustal quartz–feldspar rocks of the Aktyuz and Koyandy complexes attributed to the same stage of metamorphism at ca. 490 Ma, eclogites of these complexes are different in terms of the P–T parameters of their formation and chemical compositions. Phengite eclogites of the Aktyuz complex are derivatives of the ‘cold’ geothermal gradient (P = 21 kbar; T = 670°C; Klemd *et al.* 2014), whereas eclogites of the Koyandy complex were metamorphosed at the peak P–T conditions of the ‘hot’ gradient of 15–19 kbar and 750–850°C (Pilitsyna *et al.* 2018a) (Figure S2).

These findings may favour a distinct, oceanic tectonic setting for the formation of the Aktyuz eclogite protoliths. Protoliths of the eclogites in the Koyandy complex were already included in a sequence of continental crust prior to their HP metamorphism. Based on these observations and findings, we suggest that the Lu–Hf garnet isochron age of the near-peak stage of metamorphism for the Aktyuz eclogites should be reconsidered.

The age estimates obtained for the UHP formations of the Makbal complex in the Issyk-Kul terrane (Figure 1(b)) also appear to be ambiguous. Both age assessments of ~509–498 Ma and ~470 Ma have been interpreted as the timing of the near-peak stage of UHP metamorphism of amphibolised eclogitic rock associations (Konopelko *et al.* 2012; Rojas-Agramonte *et al.* 2013). Similarly, major discrepancies exist in the timing of UHP metamorphism for garnet–talch–chloritoid schists, as reflected by the existing ages of 502 Ma and ca. 475 Ma (Konopelko *et al.* 2012; Meyer *et al.* 2014). These age values indicate that we can constrain the timing of HP–UHP metamorphism episodes in the early Palaeozoic evolution of the CAO.

Although there is a strong consensus on the occurrence of UHP metamorphism and overprinted retrogression of the Precambrian continental crust in the Issyk-Kul, Chu-Kendykta and Zheltau terranes during the period of 509–474 Ma, the existing tectonic models are controversial and require a re-evaluation of the available age estimates and conduction of systematic, field-based geochronological and isotopic studies.

6. Conclusions

1. Migmatized kyanite-bearing garnet–mica paragneisses, garnet–kyanite paragneisses and their retrograded derivatives in the Koyandy complex within the Zheltau terrane in South Kazakhstan (SW part of the Central Asian Orogenic Belt) represent fragments of Precambrian continental crust that underwent HP re-equilibration in the latest Cambrian.
2. Prograde-stage metamorphism of the migmatized kyanite-bearing garnet–mica paragneisses occurred under P–T conditions of 9–12 kbar and 720–760°C, consistent with suprasolidus garnet growth under increased P–T and subsequent melt propagation conditions. The existence of kyanite in garnet rims constrains the lower P–T limit to 18.5 kbar and 870°C, whereas the retrograde growth of white mica is consistent with the P–T ranges of 18.5–12 kbar and 870–800°C. Detrital zircons from the granitoid leucosome of the garnet–mica paragneisses have yielded an age range between ~616 Ma and 766 Ma (SHRIMP II) for the cores. Concordant $^{206}\text{Pb}/^{238}\text{U}$ ages obtained from the rims of ten zircons and two separated zircon grains, which grew during the HP metamorphic event, correspond to ca. 485 Ma.
3. Coarse garnet grains obtained from the garnet–kyanite paragneisses of the Koyandy complex record P–T parameters of 8–9.5 kbar and 710–720°C for the prograde stage of their metamorphism. The near-peak metamorphic conditions of these rocks are determined to be P = 15–17 kbar and T = 760–810°C. Extensive kyanite growth is consistent with phengite-dehydration melting at T > 800°C and P > 10 kbar, whereas the formation of finer garnet grains indicates retrograde evolution of their host rocks at P = 12–10.5 kbar and T = ~770°C. Detrital zircon cores from the garnet–kyanite paragneisses (LA-ICP-MS) cover the age range of

593–1443 Ma, with main peaks at 611 Ma, 708 Ma, 753 Ma, 830 Ma, 914 Ma and 956 Ma. The rims of four zircon grains reveal a concordant age of ca. 487 Ma, which we interpret as the timing of the near-peak stage of HP metamorphism of their host rocks.

4. A comparison of the age peaks obtained from the paragneisses and schists of the Koyandy complex with those reported from the Kemin and Kokdzhon complexes in the adjacent Chu-Kendyktas terrane in the North Tien Shan shows strong similarities. This positive comparison allows us to suggest that sediments of the protoliths of the paragneisses and schists were possibly sourced from a single provenance area and that they were deposited during the Ediacaran–Cambrian. Among the high-grade rock formations of the Aktyuz complex in the Chu-Kendyktas terrane, eclogite-bearing garnet gneisses have yielded an age cluster of ca. 490 Ma for zircon rims. We interpret this age as the timing of HP re-equilibration. We, therefore, propose a mutual Precambrian–early Palaeozoic evolutionary trend for the high-grade metamorphic complexes in the Zheltau and Chu-Kendyktas terranes.
5. Clockwise ‘subduction-type’ P–T paths are suggested for the development of the early Palaeozoic HP metamorphic rocks in the SW part of the CAO. The zircon age estimates obtained from the HP quartz–feldspar gneisses and their retrograded derivatives in the Zheltau and Chu-Kendyktas terranes indicate that Precambrian basement rocks (Aktyuz complex; magmatic zircon cores of Tonian age of ca. 844 Ma) and Ediacaran–Cambrian sedimentary cover rocks (Kokdzhon, Kemin and Koyandy complexes; detrital zircons) were involved in the latest Cambrian subduction zone processes during the closing stages of the Palaeo-Asian Ocean.

Supplementary material. The supplementary material for this article can be found at <https://doi.org/10.1017/S0016756823000626>

Acknowledgements. The authors are grateful to Prof. Dmitry Gladkochub and an anonymous reviewer for their constructive comments and useful suggestions. A.S. is sincerely thankful to Prof. Alexander V. Sobolev for the access to the IMAF and kind support, and Dr. Andrey A. Tretyakov for his help during the fieldwork in Kazakhstan.

Funding statement. The study was supported by the Russian Science Foundation (Grant № 21-77-00055). Purchase and maintenance of Electron Probe Microanalyser in ISTERre and participation of V. Batanova were supported by the grant from the European Research Council under the European Union’s Horizon H2020 research and innovation programme (Synergy Grant MEET, grant agreement no. 856555).

Competing interests. All authors have participated in (a) conception and design, or analysis and interpretation of the data; (b) drafting the article or revising it critically for important intellectual content; and (c) approval of the final version. This manuscript has not been submitted to, nor is it under review at, another journal or other publishing venue.

Authorship. The authors have no affiliation with any organization with a direct or indirect financial interest in the subject matter discussed in the manuscript. The following authors have affiliations with organizations with direct or indirect financial interest in the subject matter discussed in the manuscript: Anfisa V. Skoblenko (Pilitsyna): Geological Institute, Russian Academy of Sciences, Pyzhevsky lane, 7a, Moscow, Russia; Nadezhda A. Kanygina: Geological Institute, Russian Academy of Sciences, Pyzhevsky lane, 7a, Moscow, Russia; Alexander S. Dubenskiy: Geological Institute, Russian Academy of Sciences, Pyzhevsky lane, 7a, Moscow, Russia; Valentina G. Batanova: Univ. Grenoble

Alpes, Univ. Savoie Mont Blanc, CNRS, IRD, IFSTTAR, ISTERre, 38000 Grenoble, France; Yildirim Dilek: Department of Geology & Environmental Earth Science, Miami University, Oxford, OH 45056, USA; Victor S. Sheshukov: Geological Institute, Russian Academy of Sciences, Pyzhevsky lane, 7a, Moscow, Russia; and Pavel A. Serov: Geological Institute of the Kola Science Centre, Russian Academy of Sciences, 184209 Apatity, Russia.

References

- Alexeiev DV, Degtyarev KE, Tretyakov AA and Kanygina NA (2021) Early Neoproterozoic (~920 Ma) granite–gneiss of the Junggar Alatau, South Kazakhstan: age substantiation based on the results of U–Th–Pb (SIMS) dating. *Doklady Earth Sciences* **496**(1), 13–16.
- Alexeiev DV, Khudoley AK and DuFrane SA (2020) Paleoproterozoic and Neoproterozoic quartzites of the Kyrgyz North Tianshan: age determination according to the results of detrital zircon dating. *Doklady Earth Sciences* **491**(2), 191–194.
- Alexeiev DV, Ryazantsev AV, Kröner A, Tretyakov AA, Xia X and Liu DY (2011) Geochemical data and zircon ages for rocks in a high-pressure belt of Chu-Yili Mountains, southern Kazakhstan: implications for the earliest stages of accretion in Kazakhstan and the Tianshan. *Journal of Asian Earth Sciences* **42**, 805–820.
- Andersen T (2002) Correction of common lead in U–Pb analyses that do not report 204Pb. *Chem Geol* **192**, 59–79.
- Andersen T (2008) ComPbCorr – software for common lead correction of U–Th–Pb analyses that do not report 204Pb. In *Laser Ablation ICP-MS in the EARTH SCIENCES: Current Practices and Outstanding Issues* (ed PJ Sylvester), vol. **40**, pp. 312–314. Vancouver: Mineralogical Association of Canada Short Course Series.
- Auzanneau E, Schmidt MW, Vielzeuf D and Connolly JAD (2010) Titanium in phengite: a geobarometer for high temperature eclogites. *Contributions to Mineralogy and Petrology* **159**, 1–24.
- Barbero E, Dilek Y, Festa A and Saccani E (2023) Ophiolites and ophiolitic mélanges: archives of Precambrian and Phanerozoic plate tectonics in orogenic belts. *Geosystems and Geoenvironments* **2**(3), 100191. <https://doi.org/10.1016/j.geogeo.2023.100191>
- Black LP, Kamo SL, Allen CM, Aleinikoff JN, Davis DW, Korsch RJ and Foudoulis C (2003) TEMORA 1: a new zircon standard for Phanerozoic U–Pb geochronology. *Chemical Geology* **200**, 155–170.
- Bouvier A, Vervoort JD and Patchett PJ (2008) The Lu–Hf and Sm–Nd isotopic composition of CHUR: constraints from unequilibrated chondrites and implications for the bulk composition of terrestrial planets. *Earth Planet Sciences Letters* **273**(1–2), 48–57.
- Carlson WD (2006) Rates of Fe, Mg, Mn, and Ca diffusion in garnet. *American Mineralogist* **91**, 1–11.
- Claoue-Long JC, Sobolev NV, Shatsky VS and Sobolev AV (1991) Zircon response to diamond pressure metamorphism in the Kokchetav massif, USSR. *Geology* **19**(7), 710–713.
- Coggon R and Holland TJB (2002) Mixing properties of phengitic micas and revised garnetphengite thermobarometers. *Journal of Metamorphic Geology* **20**, 683–696.
- Connolly JAD (1990) Multivariable phase-diagrams: an algorithm based on generalized thermodynamics. *American Journal of Science* **290**, 666–718.
- Connolly JAD (2005) Computation of phase equilibria by linear programming: a tool for geodynamic modeling and its application to subduction zone decarbonation. *Earth Planet Sciences Letter* **236**(1), 524–541.
- Degtyarev K, Yakubchuk A, Tretyakov A, Kotov A and Kovach V (2017) Precambrian geology of the Kazakh Uplands and Tien Shan: an overview. *Gondwana Research* **47**, 44–75.
- Degtyarev KE, Luchitskaya MV, Tretyakov AA, Pilitsyna AV and Yakubchuk AS *et al.* (2021) Early Paleozoic suprasubduction complexes of the North-Balkhash ophiolite zone (Central Kazakhstan): geochronology, geochemistry and implications for tectonic evolution of the Junggar-Balkhash Ocean. *Lithos* **380–381**, 105818.
- Degtyarev KE, Ryazantsev AV, Tretyakov AA, Tolmacheva TY, Yakubchuk AS, Kotov AB, Salnikova EB and Kovach VP (2013) Neoproterozoic to

- Early Paleozoic tectonic evolution of the western part of the Kyrgyz Ridge Caledonides (North Tianshan). *Geotectonics* 47(6), 377–417.
- Degtyarev KE, Tretyakov AA, Ryazantsev AV, Kotov AB, Salnikova EB, Aleksandrov PA and Anisimova IV** (2011) Stenian granitoids of the West Kyrgyz Ridge (North Tianshan): position, structure and age determination. *Doklady Earth Sciences* 441(1), 1484–1488.
- Dilek Y, Festa A, Ogawa Y and Pini GA** (2012) Chaos and geodynamics: mélanges, mélange-forming processes and their significance in the geological record. *Tectonophysics* 568–569, 1–6. <https://doi.org/10.1016/j.tecto.2012.08.002>
- Dilek Y and Furnes H** (2011) Ophiolite genesis and global tectonics: geochemical and tectonic fingerprinting of ancient oceanic lithosphere. *Geological Society of America Bulletin* 123(3–4), 387–411. <https://doi.org/10.1130/B30446.1>
- Dilek Y and Furnes H** (2014) Ophiolites and their origins. *Elements* 10(2), 93–100. <https://doi.org/10.2113/gselements.10.2.93>
- Elhoul S, Belousova E, Griffin WL, Pearson NJ and Riley SY** (2006) Trace element and isotopic composition of GJ-red zircon standard by laser ablation. *Geochimica et Cosmochimica Acta* 70, A158.
- Ganguly J and Saxena SK** (1984) Mixing properties of aluminosilicate garnets: constraints from natural and experimental data, and applications to geothermobarometry. *American Mineralogist* 69(1–2), 88–97.
- Gehrels G** (2000) Introduction to detrital zircon studies of Paleozoic and Triassic strata in western Nevada and northern California. *Geological Society of America Special Papers* 347, 1–17.
- Gehrels GE** (2012) Detrital zircon U-Pb geochronology: current methods and new opportunities. In *Tectonics of Sedimentary Basins: Recent Advances* (eds C Busby & A Azor), pp. 47–62. Chichester, UK: Wiley-Blackwell.
- Goldstein SJ and Jacobsen SB** (1988) Nd and Sr isotopic systematics of river water suspended material implications for crystal evolution. *Earth Plan Science Letters* 87, 249–265.
- He Z-Y, Zhang Z-M, Zong K-Q and Dong X** (2013) Paleoproterozoic crustal evolution of the Tarim craton: constrained by zircon U-Pb and Hf isotopes of meta-igneous rocks from Korla and Dunhuang. *Journal of Asian Earth Sciences* 78, 54–70.
- He ZY, Klemm R, Zhang ZM, Zong KQ, Sun LX, Tian ZL and Huang BT** (2015) Mesoproterozoic continental arc magmatism and crustal growth in the eastern Central Tianshan Arc Terrane of the southern Central Asian Orogenic Belt: geochronological and geochemical evidence. *Lithos* 236–237, 74–89.
- Holland T and Powell R** (2001) Calculation of phase relations involving haplogranitic melts using an internally consistent thermodynamic dataset. *Journal of Petroleum* 42, 673–683.
- Holland TJB and Powell R** (1998) An internally consistent thermodynamic data set for phases of petrological interest. *Journal of Metamorphic Geology* 16, 309–343. (у тебя в тексте выделено красным)
- Holland TJB and Powell R** (2003) Activity-composition relations for phases in petrological calculations: an asymmetric multicomponent formulation. *Contributions to Mineralogy and Petrology* 145, 492–501.
- Holland TJB and Powell R** (2011) An improved and extended internally consistent thermodynamic dataset for phases of petrological interest, involving a new equation of state for solids. *Journal of Metamorphic Geology* 29, 333–383.
- Horstwood MSA, Kosler J, Gehrels G, Jackson SE, McLean NM, Paton Ch, Pearson NJ, Sircombe K, Sylvester P, Vermeesch P, Bowring JF, Condon DJ and Schoene B** (2016) Community-derived standards for LA-ICP-MS U-(Th)-Pb geochronology – uncertainty propagation, age interpretation and data reporting. *Geostandards and Geoanalytical Research* 40, 311–332.
- Huang Z, Yuan C, Long X, Zhang Y and Du L** (2019) From breakup of Nuna to assembly of Rodinia: a link between the Chinese Central Tianshan Block and Fennoscandia. *Tectonics* 38(13), 4378–4398.
- Indares A and Dunning G** (2001) Partial melting of high-P-T metapelites from the Tshenukutish Terrane (Grenville Province): petrography and U-Pb dating. *Journal of Petrology* 42(8), 1547–1565.
- Jackson SE, Pearson NJ, Griffin WL and Belousova EA** (2004) The application of laser ablation-inductively coupled plasma-mass spectrometry to in situ U-Pb zircon geochronology. *Chemical Geology* 211, 47–69.
- Kanygina NA, Tretyakov AA, Degtyarev KE, Kovach VP, Skuzovatov SY, Pang K-N, Wang KL and Lee H-Y** (2021) Late Mesoproterozoic–early Neoproterozoic quartzite–schist sequences of the Aktau-Mointy terrane (Central Kazakhstan): provenance, crustal evolution, and implications for paleotectonic reconstruction. *Precambrian Research* 354, 106040.
- Kanygina NA, Tretyakov AA, Degtyarev KE, Pang K-N, Wang KL, Lee H-Y and Plotkina JV** (2019) First results of dating detrital zircons from the late precambrian quartzite-schist sequences of the chu block (Southern Kazakhstan). *Doklady Earth Sciences* 489(1), 1273–1276.
- Klemm R, Hegner E, Bergmann H, Pfander JA, Li JL and Hentschel F** (2014) Eclogitization of transient crust of the Aktyuz complex during late Palaeozoic plate collisions in the Northern Tianshan of Kyrgyzstan. *Gondwana Research* 26, 925–941.
- Konopelko D and Klemm R** (2016) Deciphering protoliths of the (U)HP rocks in the Makbal metamorphic complex, Kyrgyzstan: geochemistry and shrimp zircon geochronology. *European Journal of Mineralogy* 28, 1233–1253.
- Konopelko D, Kullerud K, Apayarov F, Sakiev K, Baruleva O, Ravna E and Lepekina E** (2012) SHRIMP zircon chronology of HP–UHP rocks of the Makbal metamorphic complex in the Northern Tien Shan, Kyrgyzstan. *Gondwana Research* 22(1), 300–309.
- Kovach V, Degtyarev K, Tretyakov A, Kotov A, Tolmacheva E, Wang K, Chung S, Lee H and Jahn B** (2017) Sources and provenance of the Neoproterozoic placer deposits of the Northern Kazakhstan: implication for continental growth of the western Central Asian Orogenic Belt. *Gondwana Research* 47, 28–43.
- Kröner A, Alexeiev DV, Hegner E, Rojas-Agramonte Y, Corsini M, Chao Y, Wong J, Windley BF, Liu D and Tretyakov AA** (2012) Zircon and muscovite ages, geochemistry, and Nd-Hf isotopes for the Aktyuz metamorphic terrane: evidence for an early Ordovician collisional belt in the northern Tianshan of Kyrgyzstan. *Gondwana Research* 21, 901–927.
- Kröner A, Alexeiev DV, Kovach VP, Tretyakov AA, Mikolaichuk AV, Xie H and Sobel ER** (2017b) Zircon ages, geochemistry and Nd isotopic systematics for the Palaeoproterozoic 2.3–1.8 Ga Kuilyu Complex, East Kyrgyzstan – The oldest continental basement fragment in the Tianshan orogenic belt. *Journal of Asian Earth Sciences* 135, 122–135.
- Kröner A, Alexeiev DV, Rojas-Agramonte Y, Hegner E, Wong J, Xia X, Belousova E, Mikolaichuk AV, Seltmann R, Liu D and Kiselev VV** (2013) Mesoproterozoic (Grenville-age) terranes in the Kyrgyz North Tianshan: zircon ages and Nd-Hf isotopic constraints on the origin and evolution of basement blocks in the Southern Central Asian Orogen. *Gondwana Research* 23, 272–295.
- Kröner A, Kovach V, Alexeiev DV, Wang K-L, Wong J, Degtyarev K and Kozakov I** (2017a) No excessive crustal growth in the Central Asian Orogenic Belt: further evidence from field relationships and isotopic data. *Gondwana Research* 50, 135–166.
- Kröner A, Kovach V, Belousova E, Hegner E, Armstrong R, Dolgoplova A, Seltmann R, Alexeiev DV, Hoffmann JE, Wong J, Sun M, Cai K, Wang T, Tong Y, Wilde SA, Degtyarev KE and Rytik E** (2014) Reassessment of continental growth during the accretionary history of the Central Asian Orogenic Belt. *Gondwana Research* 25, 103–125.
- Kröner A, Windley BF, Badarch G, Tomurtogoo O, Hegner E, Jahn BM, Gruschka S, Khain EV, Demoux A and Wingate MTD** (2007) Accretionary growth and crust formation in the Central Asia Orogenic Belt and comparison with the Arabian-Nubian shield. *Geological Society of America Memoir* 200, 1–29.
- Kushnareva AV, Khudoley AK, Alexeiev DV and Petrov EO** (2022) Structural setting and heterogeneous deformation of the mesoproterozoic granite-gneisses of North Tianshan with the example of the Karadjilga Massif (Kyrgyzstan). *Doklady Earth Sciences* 507(1), 855–861.
- Larionov AN, Andreichev VA and Gee DG** (2004) The Vendian alkaline igneous suite of northern Timan: ion microprobe U–Pb zircon ages of gabbros and syenite. In *The Neoproterozoic Timanide Orogen of Eastern Baltica* (eds DG Gee & V Pease), vol. 30, pp. 69–74. London: Geological Society Memoirs.
- Ludwig KR** (2005a) SQUID 1.12 a User's Manual. A Geochronological Toolkit for Microsoft Excel. Berkeley Geochronology Center, Special Publication no. 22.

- Ludwig KR (2005b) User's Manual for ISOPLOT/Ex 3.22. A Geochronological Toolkit for Microsoft Excel. Berkeley Geochronology Center, Special Publication no. 71.
- Ludwig KR (2008) Isoplot v.4.15: A Geochronological Toolkit for Microsoft Excel. Berkeley Geochronology Center, Special Publication no. 4.
- Meyer M, Klemd R, Hegner E and Konopelko D (2014) Subduction and exhumation mechanisms of ultra-high and high-pressure oceanic and continental crust at Makbal (Tianshan, Kazakhstan and Kyrgyzstan). *Journal of Metamorphic Geology* **32**, 861–884.
- Orozbaev RT, Takasu A, Bakirov AB and Sakiev KS (2010) Metamorphic history of eclogites and country rock gneisses in the Aktyuz area, Northern Tien-Shan, Kyrgyzstan: a record from initiation of subduction through to oceanic closure by continent-continent collision. *Journal of Metamorphic Geology* **28**, 317–339.
- Pilitsyna AV, Tretyakov AA, Degtyarev KE, Alifirova TA, Batanova VG, Cuthbert SJ, Kovalchuk EV and Ermolaev BV (2018b) Multi-stage metamorphic evolution and protolith reconstruction of spinel-bearing and symplectite-bearing ultramafic rocks in the Zheltau massif, Southern Kazakhstan (Central Asian Orogenic Belt). *Gondwana Research* **64**, 11–34.
- Pilitsyna AV, Tretyakov AA, Degtyarev KE, Cuthbert SJ, Batanova VG and Kovalchuk EV (2018a) Eclogites and garnet clinopyroxenites in the Anrakhai complex, Central Asian Orogenic Belt, Southern Kazakhstan: P-T evolution, protoliths and some geodynamic implications. *Journal of Asian Earth Sciences* **153**, 325–345.
- Pilitsyna AV, Tretyakov AA, Degtyarev KE, Salnikova EB, Kotov AB, Kovach VP, Wang K-L, Batanova VG, Plotkina YV, Tolmacheva EV, Ermolaev BV and Lee H-Y (2019) Early Palaeozoic metamorphism of Precambrian crust in the Zheltau terrane (Southern Kazakhstan; Central Asian Orogenic belt): P-T paths, protoliths, zircon dating and tectonic implications. *Lithos* **324–325**, 115–114.
- Raczek I, Jochum KP and Hofmann AW (2003) Neodymium and strontium isotope data for USGS reference materials BCR-1, BCR-2, BHVO-1, BHVO-2, AGV-1, AGV-2, GSP-1, GSP-2 and eight MPI-DING reference glasses. *Geostandards and Geoanalytical Research* **27**, 173–179.
- Ragozin AL, Liou JG, Shatsky VS and Sobolev NV (2009) The timing of retrograde partial melting in the Kumdy-Kol region. *Lithos* **109**, 274–284.
- Rojas-Agramonte Y, Herwartz D, Garcia-Casco A, Kröner A, Alexeiev DV, Klemd R, Buhre S and Barth M (2013) Early Palaeozoic deep subduction of continental crust in the Kyrgyz North Tianshan: evidence from Lu-Hf garnet geochronology and petrology of mafic dikes. *Contributions to Mineralogy and Petrology* **166**, 525–543.
- Rojas-Agramonte Y, Kröner A, Alexeiev DV, Jeffreys T, Khudoley AK, Wong J, Geng H, Shu L, Semiletkin SA, Mikolaichuk AV, Kiselev VV, Yang J and Seltmann R (2014) Detrital and igneous zircon ages for supracrustal rocks of the Kyrgyz Tianshan and palaeogeographic implications. *Gondwana Research* **26**, 957–974.
- Ryazantsev AV, Mikolaichuk AV, Tolmacheva TY, Degtyarev KE, Kotov AB, Nikitina OI, Mamonov EP and Zorin AE (2009) Ophiolites and island-arc complexes of Dzhalaïr-Naiman Zone and Chu-Kendykta Massifs (Southern Kazakhstan): structures, ages and formation settings. *Geodynamics of Intracontinental Orogens and Geocological Problems. Moscow-Bishkek* **4**, 53–58.
- Shatsky VS, Jagoutz E, Sobolev NV, Kozmenko OA, Parkhomenko VS and Troesch M (1999) Geochemistry and age of ultrahigh pressure metamorphic rocks from the Kokchetav mass if (Northern Kazakhstan). *Contributions to Mineralogy and Petrology* **137**, 185–205.
- Shatsky VS, Yagoutz E, Kozmenko OA, Blinichik TM and Sobolev NV (1993) Age and origin of eclogites of the Kokchetav massif (northern Kazakhstan). *Russian Geology and Geophysics* **12**, 47–58.
- Sheshukov VS, Kuzmichev AB, Dubenskiy AS, Okina OI, Degtyarev KE, Kanygina NA, Kuznetsov NB, Romanjuk TV and Lyapunov SM (2018) U-Pb zircon dating by LA-SF-ICPMS at Geological Institute GIN RAS (Moscow). 10th International Conference of the Analysis of Geological and Environmental Materials: Book of Abstracts, Sydney. 63 pp.
- Skoblenko AV and Degtyarev KE (2021) Early Paleozoic high- and ultra-high-pressure complexes in the western part of the Central Asian Orogenic Belt: ages, compositions, and geodynamic models of formation. *Petrology* **29**(3), 246–276.
- Skoblenko AV, Degtyarev KE, Kanygina NA, Pang K-N and Lee H-Y (2022) Precambrian and Early Palaeozoic metamorphic complexes in the SW part of the Central Asian Orogenic Belt: ages, compositions, regional correlations and tectonic affinities. *Gondwana Research* **105**, 117–142.
- Skoblenko AV, Kanygina NA, Tretyakov AA, Degtyarev KE, Nguyen TT, Pang K-N, Sheshukov VS and Erofeeva KG (2023) Latest Cambrian stage of evolution of Precambrian continental crust in the Aktyuz high-pressure Complex (Chu-Kendykta terrane; North Tien Shan): tectonic implications for the SW part of the Central Asian Orogenic Belt. *Journal of Geodynamics* **155**, 101955.
- Sláma J, Kosler J, Condon DJ, Crowley JL, Gerdes A, Hanchar JM, Horstwood MSA, Morris GA, Nasdala L, Norberg N, Schaltegger U, Schoene B, Tubrett MN and Whitehouse MJ (2008) Plesovice zircon – a new natural reference material for U-Pb and Hf isotopic microanalysis. *Chemical Geology* **249**, 1–35.
- Stacey JS and Kramers ID (1975) Approximation of terrestrial lead isotope evolution by a two-stage model. *Earth Planet Sciences Letter* **26**(2), 207–221.
- Steiger RH and Jäger E (1976) Subcommittee of Geochronology: conversion of the use of decay constants in geo- and cosmochronology. *Earth Planet Sciences Letter* **36**(2), 359–362.
- Sun S-s and McDonough WF (1989) Chemical and isotopic systematics of oceanic basalts: implications for mantle composition and processes. *Geological Society, London, Special Publications* **42**, 313–345.
- Tagiri M and Bakirov AB (1990) Quartz pseudomorph after coesite in garnet from a garnet-chloritoid-talc schist, northern Tien-Shan, Kirghiz SSR. *Proceedings of the Japan Academy Series* **66**, 135–139.
- Tanaka T, Togashi S, Kamioka H, Amakawa H, Kagami H, Hamamoto T, Yuhara M, Orihashi Y, Yoneda S, Shimizu H, Kunimaru T, Takahashi K, Yanagi T, Nakano T, Fujimaki H, Shinjo R, Asahara Y, Tanimizu M and Dragusanu C (2000) JNdi-1: a neodymium isotopic reference in consistency with LaJolla neodymium. *Chemical Geology* **168**, 279–281.
- Togonbaeva A, Takasu A, Bakirov AA, Sakurai T, Tagiri M, Bakirov AB and Sakiev S (2009) CHIME monazite ages of garnet-chloritoid-talc schists in the Makbal complex, Northern Kyrgyz Tien-Shan: first report of the age of the UHP etamorphism. *Journal of Mineralogical and Petrological Sciences* **104**(2), 77–81.
- Tretyakov A, Degtyarev K, Shatagin K, Kotov A, Salnikova E and Anisimova I (2015) Neoproterozoic anorogenic rhyolite - granite volcano-plutonic association of the Aktau-Mointy sialic massif (Central Kazakhstan): age, source, and paleotectonic position. *Petrology* **23**(1), 22–44.
- Tretyakov AA, Degtyarev KE, Kanygina NA and Fedorov BV (2022) The mesoproterozoic bimodal magmatism of the Ulutau Terrane, Central Kazakhstan. *Doklady Earth Sciences* **507**(2), 225–230.
- Tretyakov AA, Degtyarev KE, Kotov AB, Sa'nikova EB, Shatagin KN, Yakovleva SZ, Anisimova IV and Plotkina YV (2011b) Middle Riphean gneiss granites of the Kokchetav Massif (Northern Kazakhstan): structural position and age substantiation. *Doklady Earth Sciences* **440**(4), 511–515.
- Tretyakov AA, Kotov AB, Degtyarev KE, Salnikova EB, Shatagin KN, Yakovleva SZ and Anisimova IV (2011a) The Middle Riphean volcanogenic complex of the Kokchetav massif (northern Kazakhstan): structural position and age substantiation *Doklady Earth Sciences* **438**(5), 644–648.
- Tretyakov AA, Pilitsyna AV, Degtyarev KE, Salnikova EB, Kovach VP, Lee HY, Batanova VG, Wang K-L, Kanygina NA and Kovalchuk EV (2019) Neoproterozoic granitoid magmatism and granulite metamorphism in the Chu-Kendykta terrane (Southern Kazakhstan, Central Asian Orogenic Belt): zircon dating, Nd isotopy and tectono-magmatic evolution. *Precambrian Research* **332**, 105397.
- Van Achterbergh E, Ryan CG, Jackson SE and Griffin WL (2001) *LA ICP-MS in the Earth Sciences - Appendix 3, Data Reduction Software for LA-ICP-MS*. (ed PJ Sylvester), vol. **29**, pp. 239–243. St. John's: Mineralogical Association of Canada.
- Vermeesch P (2018) IsoplotR: a free and open toolbox for geochronology. *Geosciences Frontiers* **9**, 1479–1493
- Vielzeuf D, Baronnat A, Perchuk AL, Laporte D and Baker MB (2007) Calcium diffusivity in aluminosilicate garnets: an experimental and ATEM study. *Contributions to Mineralogy and Petrology* **154**, 153–170. (эта ли статья?)

- White RW, Powell R and Holland TJB** (2001) Calculation of partial melting equilibria in the system Na₂O-CaO-K₂O-FeO-MgO-Al₂O₃-SiO₂-H₂O (NCKFMASH). *Journal of Metamorphic Geology* **19**, 139–153.
- White RW, Powell R and Holland TJB** (2007) Progress relating to calculation of partial melting equilibria for metapelites. *Journal Of Metamorphic Geology* **25**, 511–527.
- Whitney DL and Evans BW** (2010) Abbreviations for names of rock-forming minerals. *American Mineralogist* **95**, 185–187.
- Wiedenbeck M, Alle P, Corfu F, Griffin WL, Meier M, Oberli F, von Quadt A, Roddick JC and Spiegel W** (1995) Three natural zircon standards for U-Th-Pb, Lu-Hf, trace-element and REE analyses. *Geostandards Newsletter* **19**, 1–23.
- Wiedenbeck M, Hanchar JM, Peck WH, Sylvester P, Valley J, Whitehouse M, Kronz A, Morishita Y, Nasdala L, Fiebig J, Franchi I, Girard J-P, Greenwood RC, Hinton R, Kita N, Mason PRD, Norman M, Ogasawara M, Piccoli PM, Rhede D, Satoh H, Schulz-Dobrick B, Skår Ø, Spicuzza MJ, Terada K, Tindle A, Togashi S, Vennemann T, Xie Q and Zheng Y-F** (2004) Further characterization of the 91500 zircon crystal. *Geostandards and Geoanalytical Research* **28**, 9–39.
- Williams IS** (1998) U-Th-Pb geochronology by ion microprobe. In *Applications of Microanalytical Techniques to Understanding Mineralizing Processes. Reviews in Economic Geology* (eds MA McKibben, WC Shanks III & WI Ridley), vol. 7, pp. 1–35.
- Windley BF, Alexeiev D, Xiao W, Kröner A and Badarch G** (2007) Tectonic models for accretion of the Central Asian Orogenic Belt. *Journal of the Geological Society of London* **164**, 31–47.
- Yarmolyuk VV and Degtyarev KE** (2019) Precambrian terranes of the Central Asian Orogenic belt: comparative characteristics, types, and peculiarities of tectonic evolution. *Geotectonics* **53**, 1–23.